Applied Sciences, Computing and Energy, 2025, 3(1), 40-65

A comparative assessment of Lepidolite-bearing pegmatites from Akpet and Betem areas, Southeastern Nigeria: insights from their geochemical signatures and economic potential

Benjamin Odey Omang*, Ukam Ngwu Ngwu, Uche Chukwura-Osoagba, Temple Okah Arikpo, Calvin Etongo Mbange, Godwin Terwase Kave, Bassey Edem Ephraim, Gimba Nurudeen Idris, and Etim Edidiong Joseph

Received: 19 February 2025/Accepted: 27 June 2025/Published: 01 July 2025

Abstract: *Late Proterozoic (Pan-African) pegmatites in Nigeria play host to the mineralization of lepidolite-bearing minerals such as lithium, beryl, tantalum, tourmaline, and gemstones, making it an essential resource for positioning Nigeria as a significant global pointer in solid mineral and renewable energy. This research focuses on the comparative assessment of the geochemical, and mineralogical characterization of the Lepidolite-bearing pegmatites in Akpet and Betem areas, in Cross River State, Southeastern Nigeria. Twenty samples (ten from each location) were systematically collected and analyzed using inductively coupled plasma mass spectrometry. The data were further processed using different fractional indices and multivariate statistics.* SiO_2 *recorded the highest concentration across the two locations ranging from 48.14 to 99.79% with a mean of 80.66% and 70.1 to 98.3 with a mean of 82.080%wt for Akpet and Betem area respectively.* SiO_2, Al_2O_3, K_2O, *and* Na_2O *were high while CaO, MnO, MgO, and* TiO_2 *were low in pegmatites from both areas. Trace element and rare earth element analysis revealed high concentrations of Co (78%), Rb (4%), Cu (2%), Ni (2%), and Zn (2%) in Akpet pegmatites, while Betem pegmatites were highly enriched in Rb (23%), Ba (21%), Zn (21%), and Co (13%). Results from the protolith discriminant plots of* SiO_2 *vs.* Na_2O+K_2O*-CaO and* SiO_2 *vs.* K_2O *indicate that the Akpet pegmatites exhibit a more diverse origin, possibly involving input from igneous protoliths. The discrimination plots of K/Rb vs. Rb and Ta vs. K/Cs reveal that the pegmatites from both areas were highly mineralized concerning Tantalite and Rubidium but barren to beryllium.*

Keywords: *Lepidolite, Oban massif, Akpet, Betem, pegmatites, geochemistry, Lithium, Nigeria.*

Benjamin Odey Omang
Department of Geology, University of Calabar, Calabar, Cross River State Nigeria
Email: benjaminomang@unical.edu.ng
***Orcid* id: 0000-0001-9196-3109**

Ukam Ngwu Ngwu
Department of Geology, University of Calabar, Calabar, Cross River State, Nigeria
Email: ngwuukamekuma@gmail.com

Uche Chukwura-Osoagba
Department of Geology, University of Calabar, Calabar, Cross River State, Nigeria
Email: ucheosoagba@unical.edu.ng
Orcid id: 0000-0002-3401-7340

Temple Okah Arikpo
Department of Geology, University of Calabar, Calabar, Cross River State, Nigeria
Email: arikpotemple@gmail.com
***Orcid* id: 0009-0002-9425-0125**

Calvin Etongo Mbange
Department of Geology, University of Calabar, Calabar, Cross River State, Nigeria
Email: mbangecalvin81@gmail.com

Godwin Terwase Kave
Department of Geology, University of Calabar, Calabar, Cross River State, Nigeria
Email: gkaves@yahoo.com

Bassey Edem Ephriam
Department of Geology, University of Calabar, Calabar, Cross River State, Nigeria
Email: basseyephraim@unical.edu.ng

Idris Nurudeen Gimba
Department of Geology, University of Calabar, Calabar, Cross River State, Nigeria
Email: updeen77@gmail.com

Edidiong Joseph Etim
Department of Geology, University of Calabar, Calabar, Cross River State, Nigeria
Email: deebeeetim@gmail.com

1.0 Introduction

Lepidolite, a lithium-rich mica, has gained substantial interest because of its significance as a source of lithium, a vital element in the production of batteries for electric vehicles and energy storage devices. The geological, geochemical, and mineralogical characterization of lepidolite deposits is critical for assessing their commercial value and identifying the dynamics that lead to their formation (Benchmark Mineral Intelligence Report 2023). The growing demand for lithium has increased international initiatives to seek and develop new sources of this valuable element (USGS, 2023). Granitic pegmatites, coarse-grained igneous rocks formed by magma crystallization, are usually found to include lepidolite (Gao et al., 2020, Zhang et al, 2020, Groves et al., 2022). The pegmatites are frequently found in areas with a record of substantial tectonic activity and are distinguished by their mineral complexity (Muller et al., 2022, Shen et al., 2022). In addition to typical minerals like lithium aluminosilicates (spodumene, petalite, and eucryptite), tourmaline, garnets, beryl, and pollucite, pegmatite also contains phosphates (monazite, amblygonite, lithiophyllite, and topaz), oxides (cassiterite, columbite-tantalite, rutile, uraninite, zircon, and corundum), and more (London, 2008). Li, Rb, Cs, Be, Ga, Sc, Y, REE, Sn, Nb, Ta, U, Th, Zr, and Hf are among the elements found in pegmatite. According to Linnen et al. (2012) and Dill (2015), granitic pegmatites are extremely uncommon magmas that make up sizable reserves of rare elements. Nonetheless, there is ongoing discussion over the genesis and mineralization of Li-Cs-Ta (LCT) pegmatites (Cerný & Ercit, 2005). Pegmatite formation processes are characterized at two different geological scales: the crustal scale, where the melt that forms pegmatite is formed, and the pegmatite body scale, where internal physicochemical processes result in localized concentrations of rare elements like Li, Be, Cs, and Ta. Extreme granitic fractionation is thought to be the cause of the majority of LCT-type pegmatites. Characterizing and understanding the variation and development process of lithium-rich pegmatite systems is becoming more and more important for sustainable resource management in light of the world's growing demand for lithium.

The existing research on the pegmatites in Akpet and Betem provides valuable insight, but leaves several knowledge gaps. The mineralization potential, degree of fractionation, protolith, and tectonic setting of the pegmatites in both areas is still underexplored. Also, there is no comparison between the pegmatites within these areas. This study is crucial for understanding the geochemical and mineralogical characteristics of lepidolite-bearing pegmatites in Akpet and Betem, southeastern Nigeria, which are potential sources of lithium and other valuable minerals. With the growing global demand for lithium in energy storage technologies, this research provides important insights into the composition and mineralization potential of these pegmatites, guiding both academic research and industrial applications. The study addresses a gap in existing literature by enhancing our understanding of the mineralization potential, the class of pegmatites, the protolith, degree of fractionation, and the tectonic setting. The findings provide essential data for resource management and identifying economically significant deposits.

2.0 Description of the study area

The study areas cuts across Biase Local Government Area, both located in Cross River State, Southeastern Nigeria. The area is bounded by longitude 8º 4' 5" – 8º 15' 5" E and latitude 5º21' 8" – 5º35' 0" N. The elevation in the area ranges from 50 m to 400 m above sea level. Dominant elevation

ranges in the order of 100 to 200 m above sea level, with patches ranging from 200 m to about 400 m) (*Fig.* 1).

This region is part of the Oban Massif (Nigerian Southeastern Basement Complex), characterized by Precambrian rocks that have experienced significant geological transformations (Ekwueme, 1990). The area's geology is dominated by granitic rocks with pegmatitic intrusions, where Lepidolite and other lithium-bearing minerals are hosted. The local climate is tropical, with distinct wet and dry seasons, influencing the weathering and alteration processes affecting the pegmatitic rocks.

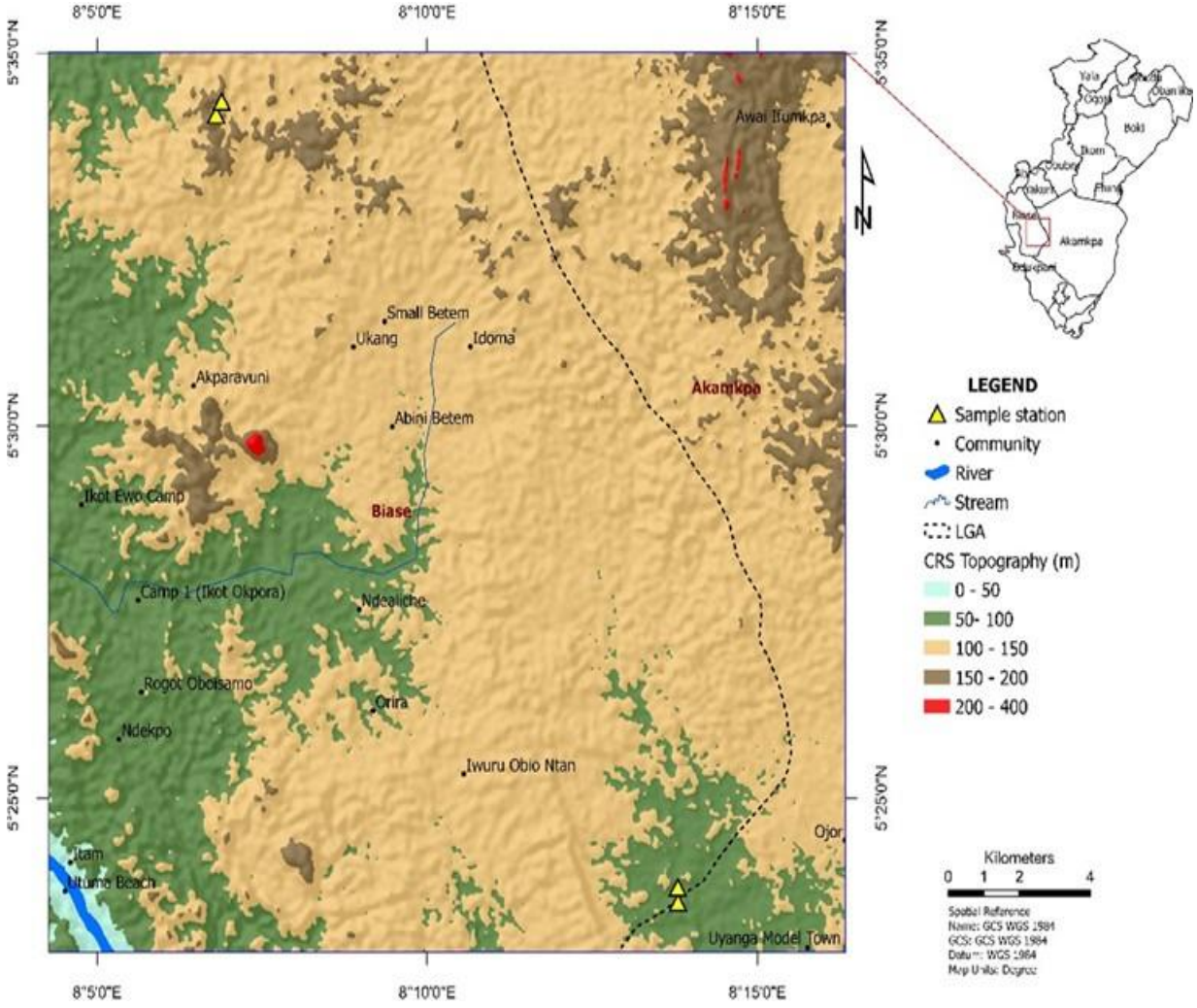

Fig.1: Location Map of the Study Area

2.1 Local geology

The study area covers Akpet and Betem (in Biase Local Government area) both situated within the Oban Massif Basement Complex in Cross River State, Southeastern Nigeria. This region is characterized by a diverse sequence of metamorphic, igneous, and sedimentary rocks, reflecting a complex geological history involving multiple phases of deformation, metamorphism, and sedimentation (*Fig.* 2). The basement rock units in the study area are composed of high-grade metamorphic and igneous rock derived from regional metamorphism of sedimentary precursors.

Biotite schist is the oldest rock unit in the study area, representing high-grade metamorphic rocks derived from the regional metamorphism of sedimentary precursors (Omang et al., 2025). The schist is characterized by its foliated texture, with

biotite, quartz, and feldspar as the dominant minerals. These rocks exhibit strong foliation and lineation, indicative of significant deformation during the metamorphic processes. Intruding the biotite
schist is the granodiorite, a coarse-grained igneous rock composed primarily of quartz, plagioclase, potassium feldspar, and biotite. The granodiorite represents an important phase of magmatism within the Oban Massif Basement Complex. It often shows varying degrees of weathering, and its intrusion has significantly influenced the structural and mineralogical characteristics of the surrounding rocks. Enclosed in the granodiorites are the lithium bearing pegmatites.

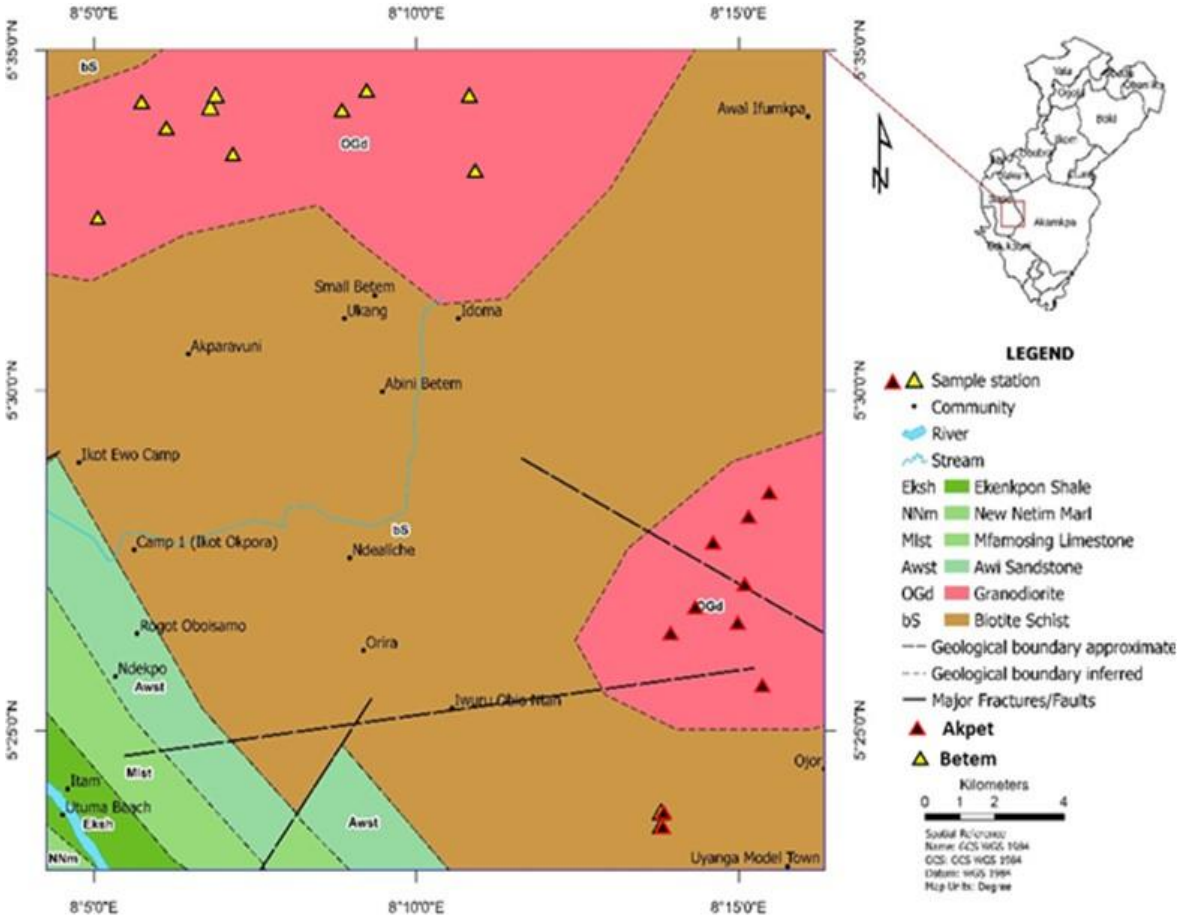

Fig. 2: Geologic map of the study area showing the different rock units and sample locations

3. 0 Materials and Methods

The materials utilized in this study for data collection and analysis include the Geologic Map of Nigeria (ver. 2010), Shovels, and Pickaxes for collecting rock samples. The samples were packed using sample bags (of polythene), and properly labelled using permanent marker. The spatial coordinates of the various sample points were established with the help of the handheld GPS device; Field Notebooks were used for documenting field observations and sample details; Protective Gear (including gloves, helmets, and boots) were worn to ensure safety in the field. Ten (10) representative pegmatite samples were collected at Akpet, and same quantity at Betem for geochemical analysis. The representative samples collected were crushed, pulverized, and subjected to acid digestion using a combination of nitric acid (HNO_3), hydrochloric acid (HCl), and hydrofluoric acid (HF) to extract elements of interest. Major, minor, and trace element concentrations were carefully measured by

Inductively Coupled Plasma-Mass Spectrometry (ICP-MS). The analysis was conducted in ACTIVATION LABORATORIES LTD, located at 41 Bittern Street, Ancaster, Ontario, Canada (with Report number: A23-10425, and Ref. no: PF15475REV).

4.0 Results and Discussion

4.1. Geochemistry of Pegmatite in Akpet and Betem

The whole-rock major and trace-element compositions for pegmatites from Akpet and Betem areas are presented in Tables 1 and 2. The different geochemical variations and tectonic diagrams are then plotted using these data.

4.1.1 Major oxide Geochemistry

Results of major oxides from Akpet and Betem areas are given in Tables 1. The variation of various oxides in the pegmatites from both areas are depicted using the bar charts in *Fig.* 3 and 4 respectively. Comparatively, among the analyzed oxides, silica oxide (SiO_2) recorded the highest concentration across the two locations with concentrations ranging from 48.14 to 99.79% with a mean of 80.66% and 70.1 to 98.3 with a mean of 82.080%wt for Akpet and Betem area respectively, and this is due to the fact that both lithologies are intermediate-felsic rocks. Generally, the percentage concentration of major oxides decreased in the order of SiO_2>Al_2O_3>Na_2O>CaO> MnO>Fe_2O_3>K_2O> P_2O_5>TiO>MgO for the Akpet area while for the Betem area it decreased in the order of SiO_2>P_2O_5>Al_2O_3>CaO>Na_2O>MnO>K_2O >TiO_2>MgO>Fe_2O_3. The elevated amounts of major elements such as SiO_2, Al_2O_3, K_2O, and Na_2O with low amounts of CaO, MnO, MgO and TiO_2 are indicative of the importance of fractional crystallization in their petrogenesis. According to Thomas & Davidson, (2012), the elevated concentration of these oxides is evident that the pegmatite formed from a granitic melt, indicating a high degree of crystallization and differentiation. High SiO_2 and Al_2O_3 content, can indicate favorable conditions for lithium concentration during the crystallization process (Meshram et al., 2021). Conversely, the low TiO_2 and MgO concentrations observed in pegmatites from both Akpet and Betem area suggest that the pegmatite is less influenced by mafic or ultramafic sources, indicating a more evolved, granitic composition (Gardiner et al., 2024). This can lead to a higher concentration of lithium-bearing minerals like lepidolite. The low levels of these oxides reflect a specific crystallization history and a more acidic environment during the formation of the pegmatite, which favors the development of lithium-rich minerals (Kesler et al., 2012). These results are consistent with that of Lepidolite concentration from Dhubri District, North East India (Meshram et al., 2021). The results are also similar to that of a study on the Petrology and geochemistry of Li-bearing pegmatites in southern Thailand where very high concentrations of SiO_2 (50.25–51.88 wt%), and Al_2O_3 (25.51–28.16 wt%) were recorded. Although compared to the pegmatites from other type localities such as Uyanga, Akwa-Ibami (I&II), Igbofia, and Iwuru (I&II) as reported by Ero et al. (2009), the mean SiO_2 content of the Akpet and Betem pegmatites are considerably lower.

4.1.2 Trace and rare earth element (REE) geochemistry

The results of trace and REE geochemistry of pegmatites from Akpet and Betem areas respectively is presented in Table 2 and 3, while the pie charts in *Fig.* 5 and 6 show the graphical variation of the trace elements within the two areas. Trace element analysis revealed an elevated concentration of Cobalt (Co) for pegmatites from the Akpet area with values ranging from 0.05 to 381ppm with a mean of 188.54ppm. An observation from the bar chart in *Fig.* 6 shows an elevated concentration for Co, Rb, Cu, Ni, and Zn with mean percentage values of 78%, 4%, 2%, and 2% respectively. The high concentration of Co indicates hydrothermal processes during the formation of pegmatites, suggesting that the pegmatite

Table 1: Descriptive statistical Result of major oxides (Wt.%) from Akpet (AKP) and Betem (BET) areas respectively

Analyte Symbol	SiO_2	Al_2O_3	Total iron ($Fe_2O_3^T$)	MnO	MgO	CaO	Na_2O	K_2O	TiO_2	P_2O_5	LOI	Total
AKP 1	98.970	1.170	0.030	0.030	0.010	0.080	0.030	0.007	0.002	0.010	96.700	197.039
AKP 2	72.010	0.860	0.040	0.040	0.030	3.290	5.960	0.011	0.120	1.020	98.710	182.091
AKP 3	48.140	13.740	0.630	0.400	0.080	1.450	0.300	0.245	0.020	1.560	99.310	165.875
AKP 4	99.790	0.610	0.010	0.010	0.010	0.020	0.030	0.005	0.010	0.180	100.500	201.175
AKP 5	99.148	0.891	0.030	0.390	0.065	1.157	5.310	0.035	0.012	0.440	99.790	207.278
AKP 6	93.341	8.825	0.090	0.036	0.024	2.691	5.489	0.176	0.110	0.500	99.880	211.171
AKP 7	54.219	12.825	0.340	0.128	0.024	1.986	5.214	0.160	0.060	0.410	87.200	162.580
AKP 8	99.149	8.429	0.010	0.230	0.041	1.652	5.161	0.164	0.091	1.459	98.200	214.595
AKP 9	60.106	1.387	0.060	0.148	0.067	0.720	3.499	0.210	0.090	0.394	98.620	165.311
AKP 10	81.743	2.130	0.110	0.222	0.019	0.146	5.818	0.013	0.020	1.327	98.700	190.254
Min	48.140	0.610	0.010	0.010	0.010	0.020	0.030	0.005	0.002	0.010		
Max	99.790	13.740	0.630	0.400	0.080	3.290	5.960	0.245	0.120	1.560		
Mean	80.660	5.087	0.135	0.164	0.037	1.319	3.681	0.103	0.056	0.731		
BET 1	73.860	1.040	0.040	0.050	0.180	6.890	0.860	0.009	0.290	0.870	89.200	173.289
BET 2	75.550	5.500	0.020	0.750	0.170	0.040	2.320	0.673	0.160	4.740	99.400	189.323
BET 3	98.300	1.380	0.010	0.010	0.010	0.020	0.030	0.009	0.010	-0.170	99.310	198.919
BET 4	70.100	6.400	0.180	0.920	0.210	0.060	2.730	0.895	0.240	6.370	89.200	177.305
BET 5	73.700	2.170	0.005	0.250	0.030	0.020	1.980	0.806	0.030	5.900	99.790	184.681
BET 6	82.930	4.400	0.230	0.660	0.139	0.760	1.380	0.550	0.040	2.870	78.700	172.680
BET 7	88.920	1.658	0.030	0.661	0.100	5.030	1.320	0.035	0.215	4.329	87.200	189.510
BET 8	85.550	2.470	0.040	0.151	0.161	5.200	0.570	0.820	0.136	1.967	98.200	195.290
BET 9	75.690	1.880	0.020	0.860	0.110	1.870	0.248	0.155	0.100	6.053	99.030	186.040
BET 10	96.170	1.366	0.040	0.660	0.076	5.238	0.250	0.102	0.047	5.349	97.200	206.510
Min	**70.100**	**1.040**	**0.005**	**0.010**	**0.010**	**0.020**	**0.030**	**0.009**	**0.010**	**-0.170**		
Max	**98.300**	**6.400**	**0.230**	**0.920**	**0.210**	**6.890**	**2.730**	**0.895**	**0.290**	**6.370**		
Mean	**82.080**	**2.827**	**0.062**	**0.499**	**0.118**	**2.515**	**1.171**	**0.407**	**0.127**	**3.827**		

Table 2: Results of trace elements and REE in pegmatites (measured in ppm) from the Akpet area

Analyte	Ag	As	Ba	Be	Bi	Br	Cd	Co	Cs	Cu	K	Ta	Hf	Hg	Ir	Mo	Ni	Pb	Rb	S
AKP 1	1.200	4.000	0.300	1.980	0.880	0.430	1.000	381.000	0.050	9.000	4.000	0.990	0.400	0.890	4.000	6.000	12.000	4.300	18.220	0.005
AKP 2	1.800	69.000	112.000	1.450	0.760	0.430	2.000	112.000	45.000	7.000	5.000	8.000	0.400	0.880	4.220	1.900	7.000	22.000	960.000	0.002
AKP 3	5.000	21.000	0.450	2.010	0.990	0.550	0.454	0.050	35.000	11.000	9.000	0.965	19.000	275.000	0.009	55.000	9.000	14.000	2770.000	13.000
AKP 4	1.880	3.000	0.980	1.773	0.650	0.430	1.000	163.000	0.600	5.000	5.000	4.000	0.400	0.880	4.500	3.000	5.000	7.000	19.220	0.003
AKP 5	3.720	14.392	65.782	1.968	0.696	0.521	0.572	377.448	16.037	7.686	8.000	3.468	2.724	162.458	0.296	35.909	10.309	17.799	285.111	7.408
AKP 6	4.423	12.338	9.487	1.785	0.822	0.507	0.962	80.610	32.062	8.368	4.800	6.881	4.140	211.549	1.942	28.926	10.544	15.987	1719.326	4.742
AKP 7	4.560	38.650	30.698	1.719	0.962	0.467	1.463	347.975	40.926	6.709	3.200	7.662	13.764	133.287	3.809	15.778	8.361	20.504	2282.139	12.182
AKP 8	4.970	45.179	103.251	1.511	0.804	0.491	1.626	216.042	25.426	8.892	12.400	1.577	2.970	23.505	4.025	53.247	8.805	4.611	1805.769	7.471
AKP 9	1.921	22.745	105.503	1.478	0.934	0.433	0.804	67.031	33.361	7.206	5.300	4.580	1.920	189.696	3.197	26.929	10.863	10.267	1260.306	10.053
AKP 10	4.908	46.936	72.519	1.477	0.735	0.439	0.942	140.310	34.665	10.105	4.900	1.227	5.197	48.597	3.456	52.299	7.990	21.810	1896.921	3.020
Min	1.200	3.000	0.300	1.450	0.650	0.430	0.454	0.050	0.050	5.000	3.200	0.965	0.400	0.880	0.009	1.900	5.000	4.300	18.220	0.002
Max	5.000	69.000	112.000	2.010	0.990	0.550	2.000	381.000	45.000	11.000	12.400	8.000	19.000	275.000	4.500	55.000	12.000	22.000	2770.000	13.000
Mean	3.438	27.724	50.097	1.715	0.823	0.470	1.082	188.547	26.313	8.097	6.160	3.935	5.092	104.674	2.945	27.899	8.987	13.828	1301.701	5.789

Table 2: Results of trace elements and REE in pegmatites (measured in ppm) from the Akpet area (Contd.)

Analyte	Sb	Sc	Se	Sr	Ta	Th	U	V	W	Y	Zn	Zr	La	Ce	Nd	Sm	Eu	Tb	Yb	Lu
AKP 1	0.300	0.200	0.220	5.000	0.990	0.500	0.320	6.000	2.100	0.440	10.000	4.000	0.900	2.220	3.000	0.200	0.200	0.400	0.100	0.010
AKP 2	0.900	0.800	0.120	28.000	8.000	0.430	1.500	3.440	2.800	0.930	31.000	7.000	1.400	3.000	4.000	0.300	0.100	0.300	0.300	0.020
AKP 3	0.220	0.320	2.300	3.200	0.965	0.670	3.020	2.110	2.330	1.220	34.000	331.000	21.300	2.330	33.200	4.550	0.120	0.330	2.030	0.340
AKP 4	0.110	0.100	2.900	1.800	4.000	0.430	0.410	3.440	2.890	0.340	2.000	5.000	0.120	2.120	4.220	0.210	0.200	0.410	0.090	0.003
AKP 5	0.156	0.316	2.356	20.917	3.468	0.647	2.974	3.730	2.790	0.527	29.906	294.364	19.487	2.495	20.054	0.508	0.105	0.341	1.615	0.320
AKP 6	0.511	0.205	2.177	11.156	6.881	0.533	2.740	5.486	2.673	0.513	18.297	9.092	21.210	2.314	10.932	1.581	0.108	0.308	0.560	0.171
AKP 7	0.763	0.770	2.847	16.617	7.662	0.655	1.036	5.844	2.132	0.627	21.642	204.207	9.004	2.565	29.819	2.208	0.139	0.369	0.292	0.222
AKP 8	0.649	0.469	1.372	13.921	1.577	0.654	1.853	2.357	2.407	1.119	21.913	233.588	8.902	2.180	26.093	3.832	0.144	0.349	0.959	0.292
AKP 9	0.717	0.392	0.650	9.305	4.580	0.538	2.419	5.647	2.120	0.891	15.480	94.850	9.497	2.908	11.621	2.750	0.197	0.322	1.791	0.153
AKP 10	0.819	0.709	2.293	4.182	1.227	0.575	2.304	2.658	2.792	0.555	23.065	288.058	6.461	2.951	32.458	2.622	0.159	0.369	1.017	0.010
Min	0.110	0.100	0.120	1.800	0.965	0.430	0.320	2.110	2.100	0.340	2.000	4.000	0.120	2.120	3.000	0.200	0.100	0.300	0.090	0.003
Max	0.900	0.800	2.900	28.000	8.000	0.670	3.020	6.000	2.890	1.220	34.000	331.000	21.300	3.000	33.200	4.550	0.200	0.410	2.030	0.340
Mean	0.514	0.428	1.723	11.410	3.935	0.563	1.858	4.071	2.504	0.716	20.730	147.116	9.828	2.508	17.540	1.876	0.147	0.350	0.875	0.154

Table 3: Results of trace elements and REE in pegmatites (measured in ppm) from the Betem area

Analyte	Ag	As	Ba	Be	Bi	Br	Cd	Co	Cs	Cu	K	Ta	Hf	Hg	Ir	Mo	Ni	Pb	Rb	S
BET 1	1.990	43.000	248.000	3.000	0.550	0.320	0.870	152.000	25.000	6.000	6.200	35.000	2.000	0.450	3.330	4.000	8.000	4.500	270.000	0.003
BET 2	1.030	151.000	16.000	0.870	0.780	0.120	9.000	281.000	26.500	20.000	5.200	3.000	3.500	0.660	4.220	1.700	30.000	12.000	200.000	0.005
BET 3	2.000	36.000	0.500	0.990	0.660	0.500	2.000	393.000	0.040	11.000	2.220	0.770	0.400	0.890	3.890	7.000	11.000	4.800	17.030	0.003
BET 4	1.990	309.000	18.000	1.650	0.550	0.310	25.000	277.000	23.900	40.000	3.400	7.000	3.900	0.770	4.600	1.550	35.000	16.000	170.000	0.004
BET 5	1.340	55.000	2.000	1.880	0.230	0.210	0.550	165.000	5.800	5.000	6.200	0.670	5.600	0.660	4.700	1.780	13.000	13.000	130.000	0.007
BET 6	1.641	304.900	101.840	1.034	0.278	0.280	6.860	363.900	26.489	28.290	6.200	31.790	5.000	0.640	4.245	3.011	17.851	7.995	201.863	0.006
BET 7	1.696	234.395	237.516	2.840	0.270	0.270	7.674	301.300	16.952	18.085	5.200	18.363	4.219	0.722	4.451	4.770	28.772	14.506	235.040	0.006
BET 8	1.056	97.381	191.417	1.100	0.600	0.315	23.360	198.530	1.597	26.983	12.300	5.109	3.819	0.456	3.582	2.006	8.626	4.593	85.582	0.004
BET 9	1.125	84.240	85.245	2.347	0.371	0.193	5.250	261.344	7.371	25.835	10.220	12.660	1.136	0.694	3.611	6.089	28.347	12.584	161.468	0.006
BET 10	1.423	197.472	164.185	1.878	0.434	0.311	22.983	226.600	24.588	16.608	9.220	12.152	4.482	0.825	4.457	2.027	26.834	9.126	178.002	0.006
Min	1.030	36.000	0.500	0.870	0.230	0.120	0.550	152.000	0.040	5.000	2.220	0.670	0.400	0.450	3.330	1.550	8.000	4.500	17.030	0.003
Max	2.000	309.000	248.000	3.000	0.780	0.500	25.000	393.000	26.500	40.000	12.300	35.000	5.600	0.890	4.700	7.000	35.000	16.000	270.000	0.007
Mean	1.529	151.243	106.471	1.760	0.473	0.284	10.356	261.974	15.824	19.781	6.636	12.652	3.406	0.677	4.109	3.393	20.743	9.910	164.899	0.005

Table 3: Results of trace elements and REE in pegmatites (measured in ppm) from the Betem area (Contd.)

Analyte	Sb	Sc	Se	Sr	Ta	Th	U	V	W	Y	Zn	Zr	La	Ce	Nd	Sm	Eu	Tb	Yb	Lu
BET 1	0.100	0.800	1.550	30.000	35.000	1.200	4.600	8.000	2.500	1.000	242.000	12.000	2.200	2.330	4.000	0.900	0.088	0.300	0.100	0.040
BET 2	0.900	9.300	2.000	20.000	3.000	5.500	3.800	130.000	2.800	12.000	57.000	126.000	33.600	66.000	32.000	6.600	1.000	0.500	0.900	0.100
BET 3	0.200	0.200	2.000	3.000	0.770	0.040	0.440	6.000	2.600	0.830	4.000	4.000	1.000	2.330	4.230	0.200	0.066	0.490	0.220	0.030
BET 4	0.400	13.100	2.500	27.000	7.000	6.400	6.000	165.000	2.120	17.000	65.000	192.000	30.300	63.000	37.000	6.400	1.000	0.340	1.400	0.090
BET 5	0.300	7.300	2.100	34.000	0.670	8.100	2.100	106.000	1.990	31.000	12.000	244.000	43.400	79.000	41.000	7.500	1.000	0.500	2.500	0.260
BET 6	0.330	4.114	2.349	6.786	31.796	5.880	3.419	89.112	2.335	23.042	65.370	198.458	6.927	3.992	19.885	4.855	0.825	0.446	0.767	0.208
BET 7	0.846	7.279	2.315	5.141	18.363	2.552	0.902	109.366	2.196	26.847	92.593	68.097	1.921	73.901	7.603	2.099	0.741	0.322	1.346	0.256
BET 8	0.713	10.400	2.426	20.970	5.109	5.231	2.917	35.774	2.763	9.092	189.595	81.183	23.354	21.707	21.933	1.617	0.084	0.486	0.495	0.139
BET 9	0.828	12.259	1.825	27.268	12.660	3.507	5.894	53.766	2.720	13.726	238.068	13.898	6.469	70.616	29.693	4.302	0.162	0.415	1.932	0.237
BET 10	0.839	5.834	1.986	33.534	12.152	2.525	4.671	50.990	2.768	28.910	185.097	66.676	20.047	19.466	8.600	6.506	0.999	0.391	0.905	0.065
Min	0.100	0.200	1.550	3.000	0.670	0.040	0.440	6.000	1.990	0.830	4.000	4.000	1.000	2.330	4.000	0.200	0.066	0.300	0.100	0.030
Max	0.900	13.100	2.500	34.000	35.000	8.100	6.000	165.000	2.800	31.000	242.000	244.000	43.400	79.000	41.000	7.500	1.000	0.500	2.500	0.260
Mean	0.546	7.059	2.105	20.770	12.652	4.094	3.474	75.401	2.479	16.345	115.072	100.631	16.922	40.234	20.595	4.098	0.596	0.419	1.056	0.142

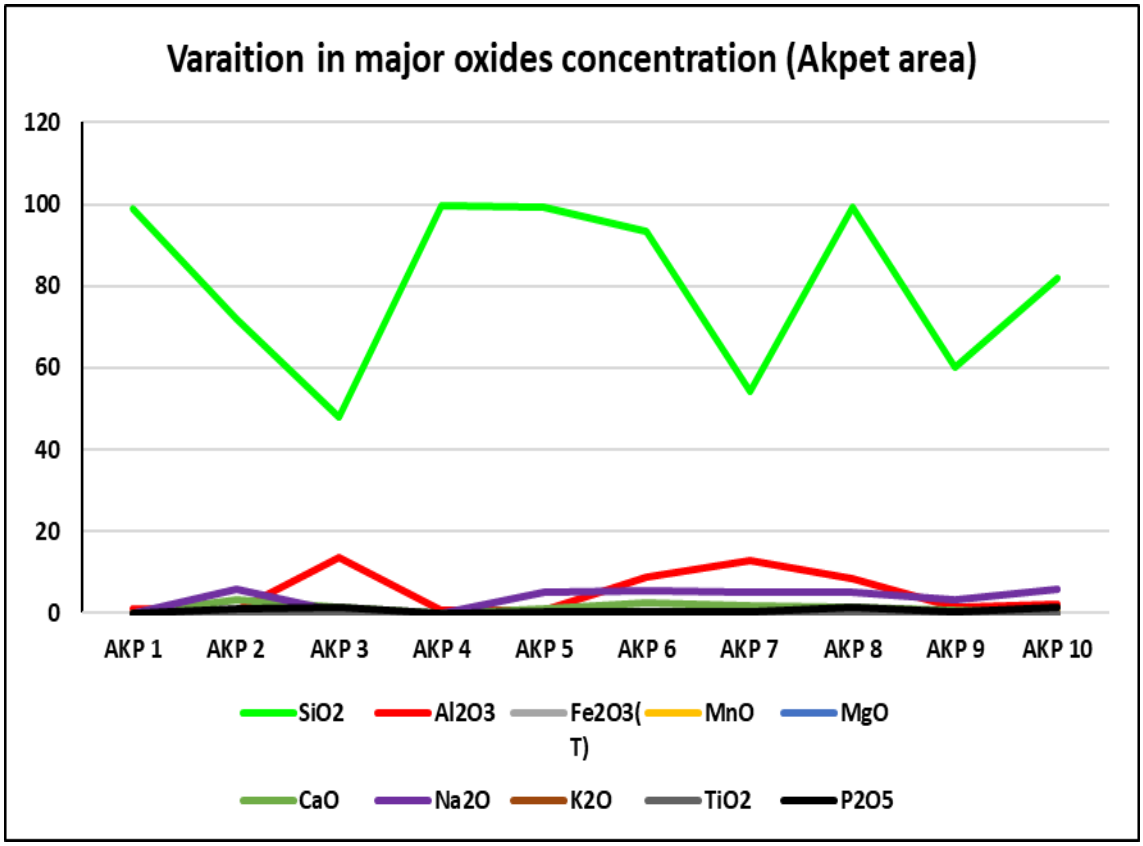

Fig. 3 :Graphical variation of major oxides in pegmatites from Akpet (AKP)

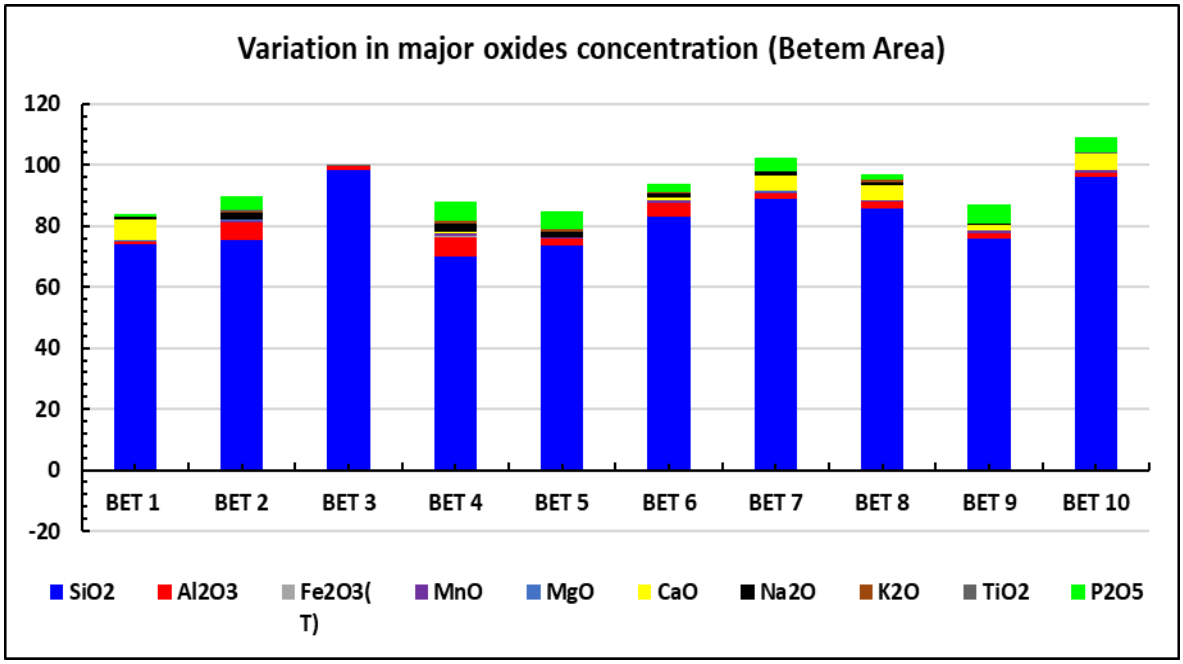

Fig. 4: Graphical variation of major oxides in pegmatites from Betem (BET)

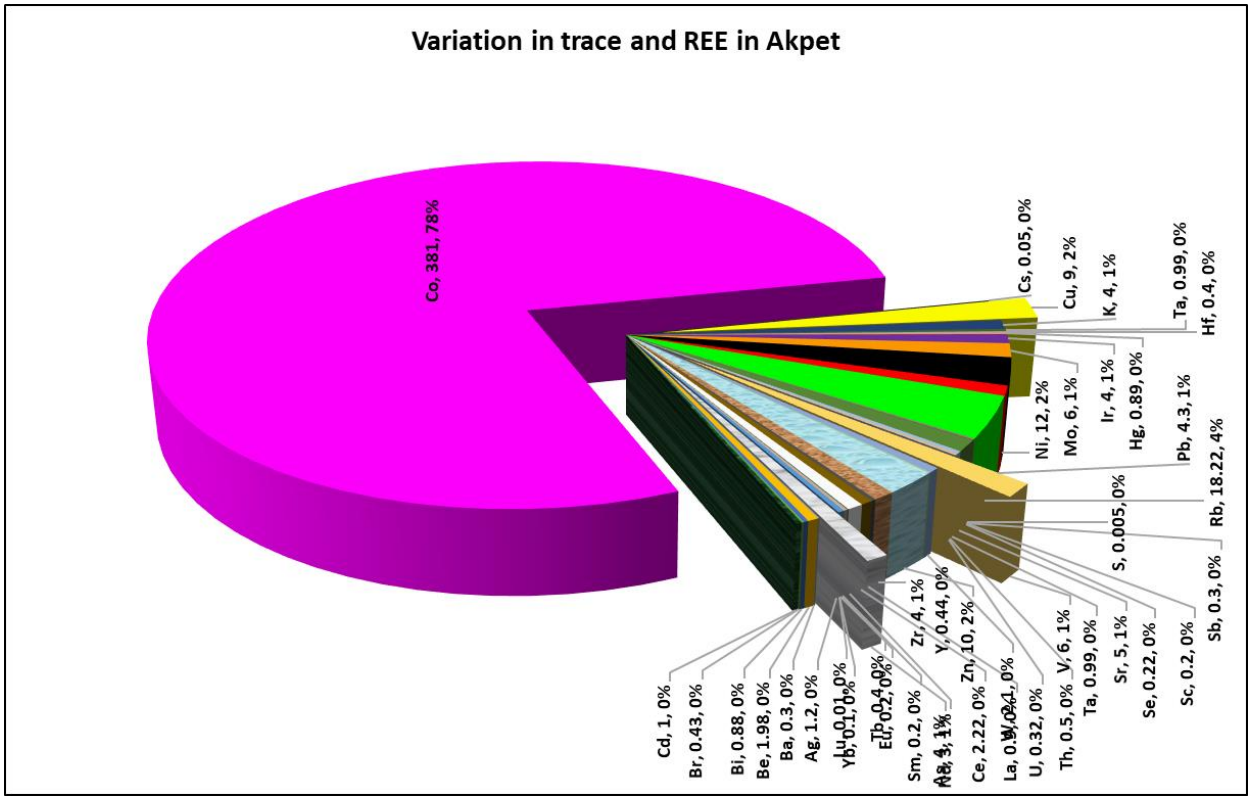

Fig. 5: Bar chart showing the variation of trace elements in pegmatites from the Akpet (AKP) area

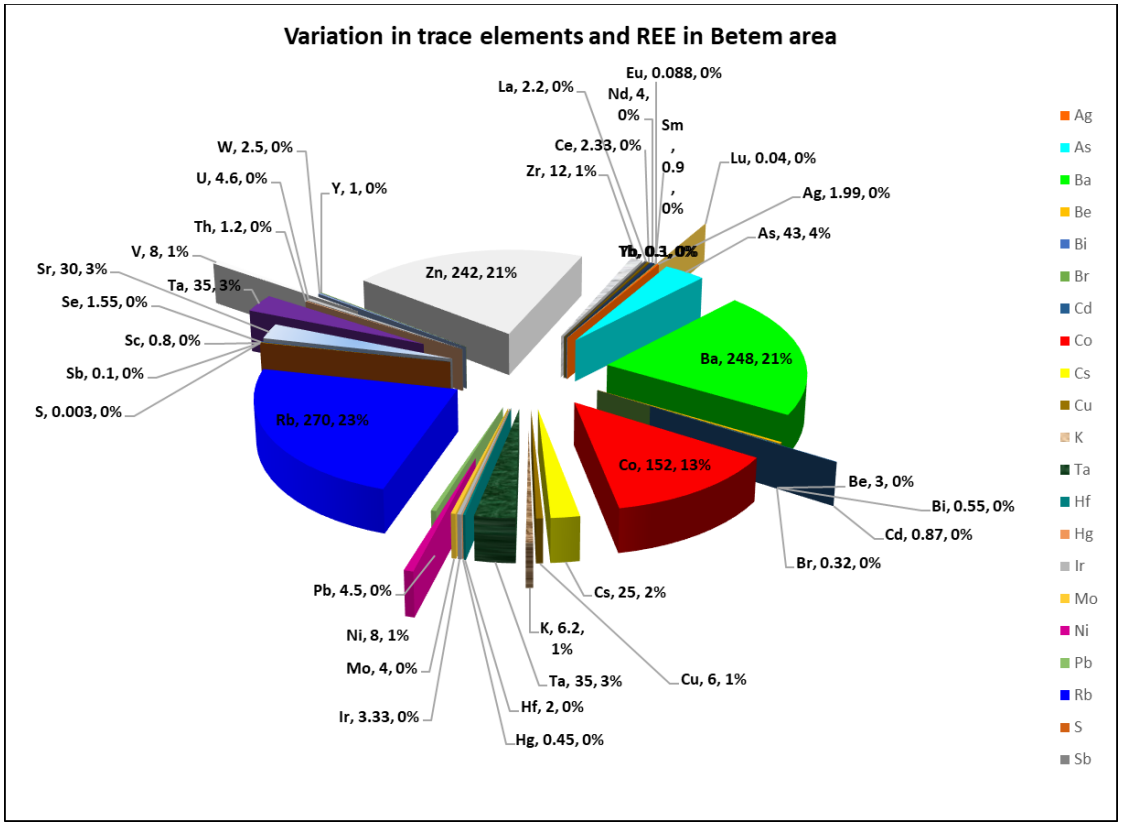

Fig.6 ; Bar charts showing the variation trace elements and REE in pegmatites from Betem area

may have formed from a volatile-rich melt that underwent significant differentiation (Li et al., 2024). Besides, Lepidolite often contains Co as a trace element. Its presence can indicate the potential for cobalt-rich mineralization in the surrounding rock (Dharmapriya et al., 2025). Rb is a lithophile element commonly associated with the crystallization of pegmatites (Ercit et al., 2005). Its moderate concentration indicates the degree of differentiation of the pegmatitic melt serving as a marker for the evolution of the parental magma. Ni concentrations correlate with a study on the occurrence of Nickel-bearing minerals in Western Australia that the presence of nickel-bearing minerals is often associated with ultramafic rocks and can suggest interesting geochemical processes in pegmatite formation (Taylor, 1974).

The trace and REE from Betem showed a higher variability in concentration compared to those from Akpet (*Fig.* 6). Results from ICP-MS showed an elevated variable concentration of Rb, Ba, Zn, and Co with mean values of 270ppm (23%), 248ppm (21%), 242ppm (21%), and 152ppm (13%) respectively (as shown in Table 2). The presence of Rb and Ba are often associated with granitic rocks and may suggest a late-stage differentiation of the magma (El Bouseily, & El Sokkary, 1975).

4.1.3 Statistical relationship between major oxides, trace elements, and REE in pegmatites

In the present study, multivariate statistical analysis was carried out to assess the relationship between the geochemistry of major oxides and trace elements of pegmatites from the Akpet and Betem areas. The analysis was carried out using the principal component analysis (PCA). The significant principal component (PCs) was considered at > 0.5, medium principal loadings were considered between 0.5 and 0.75, while high loading was taken at > 0.75 (Cui et al., 2011). Results of the unrotated PCs for both Akpet and Betem areas are presented in Tables 4 and 5 while *Figs.* 7 and 8, represents 3-D biplots showing the relationship between highly correlated variables for Akpet and Betem respectively.

The PCA results extracted at total of nine PCs respectively for the Akpet and Betem area. For the Akpet area, the PC explained a cumulative variance (CV) of 100% of the dataset, with 34.8%, 20.7%, 10.4%, 9.2%, 7.3%, 5.4%, 4.8%, 4.0%, and 3.06% for PC1, PC2, PC3, PC4, PC5, PC6, PC7, PC8, and PC9.

The greater the number of PCs extracted in a particular iteration of principal components, the greater the degree of variability in the geochemical composition of a particular environmental system (Omeka et al., 2023; Krishna-Kumar et al. (2014). The high number of PCs extracted for the trace elements and major oxides in Akpet pegmatites indicates that a wider range of geochemical factors may have influenced their geochemistry and tectonic evolution. This validates the results from the Geochemical ratios and plots. The positions of variables in 3D rotated space (*Fig.* 7) revealed that SiO_2 is a member in a homogeneous significant observation group (at >0.5) formed by fourteen variables (SiO_2, Ni, Zr, Be, total iron ($Fe_2O_3^T$), MnO, Ba, Cu, Hg, MnO, MgO, Yb, K, K_2O). This validates earlier results from geochemical plots. The positive significant loading of SiO_2 confirms that the pegmatite formed from a granitic melt, indicating a high degree of crystallization and differentiation. The significant positive loading of SiO_2, Zn, and Ni agrees with previous results (in this study) that they indicate favorable conditions for lithium concentration during the crystallization process (Meshram et al., 2021).

For the Betem area, the PC explained a cumulative variance (CV) of 100% of the dataset, with 33.13%, 15.8%, 11.9%, 10.9%, 8.4%, 6.9%, 5.01%, 4.2%, and 3.4% for PC1, PC2, PC3, PC4, PC5, PC6, PC7, PC8, and PC9. Similar to the Akpet pegmatites, the high number of PCs extracted indicates high geochemical and tectonic factors as signatures for the mineralization of

Table 4: Rotated Principal component summary of parameters from Akpet pegmatites

Component	Initial Eigenvalues		
	Total	**% of Variance**	**Cumulative %**
1	17.446	34.891	34.891
2	10.367	20.734	55.625
3	5.208	10.415	66.04
4	4.603	9.207	75.247
5	3.662	7.323	82.57
6	2.73	5.461	88.031
7	2.427	4.854	92.885
8	2.027	4.054	96.939
9	1.531	3.061	100

Table 5: Rotated Principal component summary of parameters from Betem pegmatites

Principal Component	Initial Eigenvalues		
	Total	**% of Variance**	**Cumulative %**
1	16.568	33.136	33.136
2	7.918	15.835	48.971
3	5.982	11.964	60.935
4	5.452	10.903	71.838
5	4.234	8.469	80.307
6	3.456	6.911	87.218
7	2.506	5.012	92.23
8	2.148	4.297	96.527
9	1.737	3.473	100

lepidolite-bearing lithium in the Betem area. In contrast to the results from the Akpet area, the positions of variables in 3D rotated space (*Fig.* 8) revealed that Co and Rb are members in a homogeneous significant observation group (at >0.5) formed by sixteen variables (TiO_2, Al_2O_3, Be, Co, As, NaO, Rb, Pb, Ni, P_2O_5, MnO, Hg, Sc, Yb, Cs, Ce). The positive significant loading of Co and Rb reaffirms hydrothermal processes during the formation of pegmatites, which validates earlier findings that the pegmatite from the Betem area may have formed from a volatile-rich melt that underwent significant differentiation (Li et al., 2024).

4.2 Classification of Pegmatites

Various oxide ratios were calculated to classify and compare the pegmatites from the Akpet and Betem areas. Results of the various ionic ratios are presented in Table 6 and 7, while the geochemical discriminant plots and Total Alkali silica (TAS), and Modified Alkali-Lime index (MALI) plots from the calculated oxide ratios are presented in *Figs.* 7 and 8.

The SiO_2 vs. K_2O binary plot (*Fig.* 9A) shows that pegmatites from both Akpet and Betem fall within the calc-alkaline field, indicating that they are related to magmas typically associated with convergent plate margins (Peccerillo & Taylor, 1976). This suggests that their parental melts were likely derived from a subduction-modified lithospheric source (Aydin, 2008). However, the SiO_2 vs. Na_2O+K_2O-CaO Modified Alkali-Lime index (MALI) plot of Frost et al. (2001) (*Fig.*

9B) reveals a slight difference between the two regions. According to the MALI classification index, those suites that have an alkali-lime index of > 61 are calcic, those where it is between 56 and 61 are calc-alkalic, those where it is between 51 and 56 are alkali-calcic and those where it is < 51 are alkalic. While pegmatites from both Akpet and Betem plot within the calcic-alkali and alkalic fields, a larger proportion of samples from Akpet

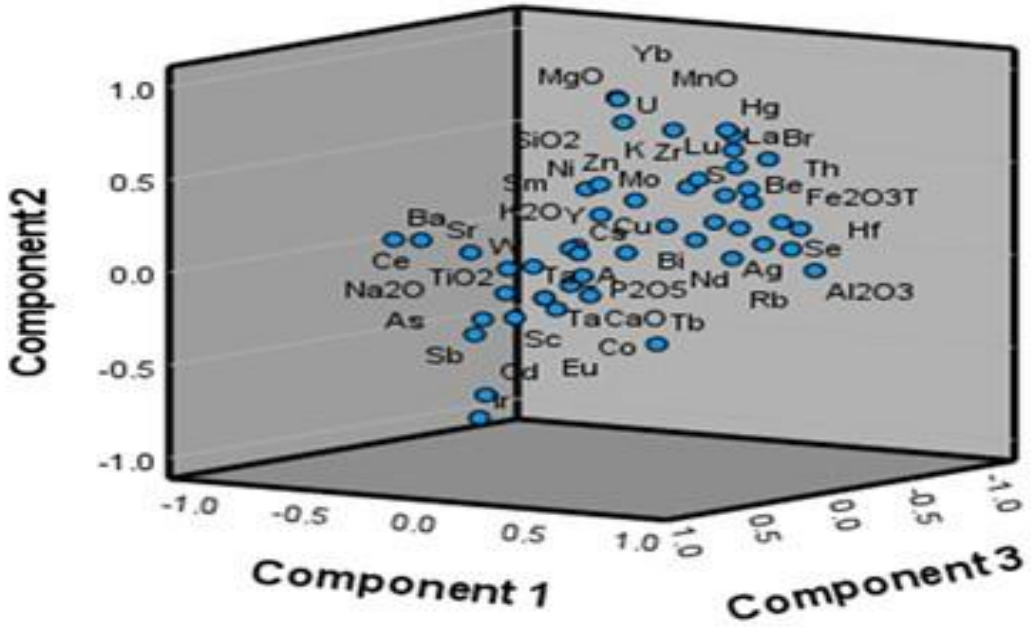

Fig. 7: 3D biplots showing the relationship between highly correlated variables for Akpet pegmatites

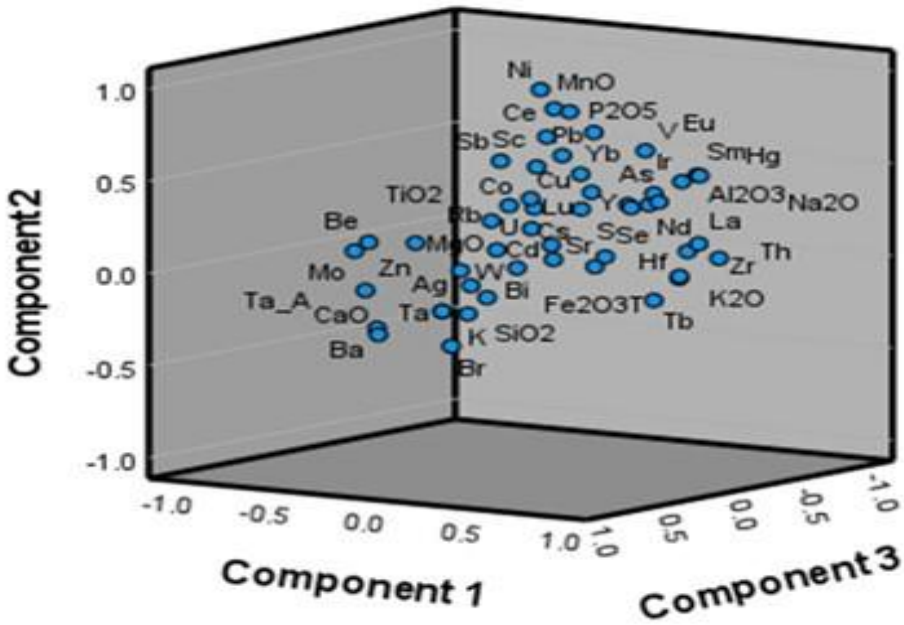

Fig. 8: 3D biplots showing the relationship between highly correlated variables for Akpet and Betem respective

Table 6: Indices of fractionation for the pegmatites in Akpet

Sample	ACR	ANR	FM	CNR	FMR	NKC	CMF	CFMT	CA	ACNK	NTR	KSR
AKP 1	14.662	39.007	0.040	2.673	0.750	-0.043	0.120	0.122	1.250	10.000	10.000	0.000
AKP 2	6.232	0.155	0.070	0.563	0.571	2.681	3.360	3.480	4.150	0.093	216.279	0.000
AKP 3	10.021	46.045	0.710	5.078	0.887	-0.905	2.160	2.180	15.190	6.887	0.110	0.005
AKP 4	30.535	20.338	0.020	0.672	0.500	0.015	0.040	0.050	0.630	11.091	0.025	0.000
AKP 5	6.119	0.203	0.096	0.253	0.314	4.192	1.251	1.266	2.047	0.137	0.216	0.000
AKP 6	8.944	1.784	0.114	0.666	0.789	2.974	2.806	2.919	11.517	1.056	0.510	0.002
AKP 7	11.832	2.620	0.364	0.541	0.934	3.389	2.350	2.415	14.811	1.742	2.101	0.003
AKP 8	10.426	1.797	0.051	0.484	0.197	3.672	1.703	1.801	10.080	1.208	1.880	0.001
AKP 9	5.640	0.612	0.127	0.422	0.472	2.994	0.848	0.939	2.108	0.313	0.221	0.004
AKP 10	20.329	0.379	0.129	0.038	0.851	5.685	0.276	0.306	2.277	0.356	5.981	0.000

Key; **ACR** = Al_2O_3 / (CaO + Na_2O + K_2O), **ANR** = Al_2O_3 / (Na_2O + K_2O), **FM** = Fe_2O_3 + MgO, **CNR** = CaO / (Na_2O + K_2O), **FMR** = Fe_2O_3 / (Fe_2O_3 + MgO), **NKC** = Na_2O + K_2O – CaO, **CMF** = CaO + MgO + FeO, **CFMT** = CaO + $Fe_2O_3^T$ + MgO + TiO_2, **CA** = CaO + Al_2O_3, **ACNK** = Al / (Ca + Na + K), **NTR** = Nb / Ta, **KSR** = K_2O / SiO_2

Table 6: Indices of fractionation for the pegmatites in Akpet (Contd.)

Sample	ANK	NKC	CFMT	FMA	FMB	TZR	NTZ	SRRB	BARB	RB30	TA3
AKP 1	31.622	0.000	0.098	0.641	0.019	0.000	0.065	4.386	0.029	2.333	9.000
AKP 2	0.144	0.037	0.839	0.664	3.680	0.000	0.674	0.136	0.043	4.667	1.290
AKP 3	25.211	-0.019	0.143	0.065	0.019	0.000	0.002	0.036	0.041	44.000	114.000
AKP 4	17.429	0.000	0.079	0.820	0.025	0.003	0.006	0.007	0.002	255.000	465.000
AKP 5	0.167	0.042	0.619	0.352	1.545	0.000	0.005	0.018	0.006	85.600	153.000
AKP 6	1.558	0.032	0.253	0.089	0.442	0.000	0.002	0.045	0.008	152.540	418.468
AKP 7	2.386	0.063	0.163	0.073	0.356	0.001	0.028	0.051	0.010	168.735	61.426

AKP 8	1.582	0.037	0.179	0.023	0.110	0.001	0.015	0.004	0.006	218.291	140.808
AKP 9	0.373	0.050	0.445	0.340	0.771	0.000	0.001	0.015	0.007	215.410	174.429
AKP 10	0.365	0.070	0.134	0.400	2.244	0.000	0.034	0.013	0.004	162.139	32.348

Keys ; **ANK** = Al / (Na + K), **NKC** = (Na_2O + K_2O – CaO) / SiO_2, **CFMT** = (CaO + $Fe_2O_3^T$ + MgO + TiO_2) / (CaO + Al_2O_3), **FMA** = (Fe_2O_3 / (Fe_2O_3 + MgO)) / Al_2O_3, **FMA** = (Fe_2O_3 / (Fe_2O_3 + MgO)) / (Al_2O_3 + Na_2O + K_2O), **TZR** = TiO_2 / Zr, **NTZ** = Nb / Ta / Zr, **SRRB** = Sr / Rb, **BARB** = Ba / Rb, **RB30** = Rb / 30, **TA3** = Ta × 3

Table 7: Indices of fractionation for the pegmatites in Betem

Sample	ACR	ANR	FMM	CNR	FMR	NKC	CMF	CFTM	CAL	ACNK	NTR	KSR
BET 1	1.020	1.218	0.220	8.021	0.182	-6.021	7.110	7.400	7.930	0.134	0.114	0.000
BET 2	140.493	3.044	0.190	0.690	0.105	2.953	0.230	0.390	5.540	1.813	10.667	0.009
BET 3	69.039	46.009	0.020	0.676	0.500	0.019	0.040	0.050	1.400	23.390	5.494	0.000
BET 4	110.292	3.239	0.390	0.917	0.462	3.565	0.450	0.690	6.460	1.737	5.286	0.013
BET 5	111.286	1.902	0.035	0.816	0.143	2.766	0.055	0.085	2.190	0.773	61.194	0.011
BET 6	7.694	3.725	0.366	1.109	0.628	1.181	1.132	1.172	5.166	1.622	0.625	0.007
BET 7	1.688	1.289	0.131	3.844	0.230	-3.681	5.170	5.385	6.698	0.259	0.414	0.000
BET 8	1.877	5.156	0.201	9.931	0.199	-3.806	5.409	5.545	7.683	0.375	4.293	0.010
BET 9	1.414	7.742	0.135	7.675	0.148	-1.467	2.007	2.107	3.759	0.830	2.345	0.002
BET 10	0.620	5.431	0.116	20.522	0.344	-4.870	5.354	5.401	6.605	0.244	0.708	0.001

Keys; **ACR** = Al_2O_3 / (CaO + Na_2O + K_2O), **ANR** = Al_2O_3 / (Na_2O + K_2O), **FMM** = Fe_2O_3 + MgO, **CNR** = CaO / (Na_2O + K_2O), **FMR** = Fe_2O_3 / (Fe_2O_3 + MgO), **NKC** = Na_2O + K_2O – CaO, **CMF** = CaO + MgO + FeO, **CFTM** = CaO + Fe_2O_3T + MgO + TiO_2, **CAL** = CaO + Al_2O_3, **ACNK** = Al / (Ca + Na + K), **NTR** = Nb / Ta, **KSR** = K_2O / SiO_2

Table 7: Indices of fractionation for the pegmatites in Betem (Contd.)

Sample	ANK	NKCS	CFTMCA	FMAA	FMANK	TZR	NTZ	SRRB	BARB	RB30	TA3
BET 1	1.197	-0.082	0.933	0.175	0.149	0.024	0.010	0.111	0.919	9.000	105.000
BET 2	1.838	0.039	0.070	0.019	0.035	0.001	0.085	0.100	0.080	6.667	9.000
BET 3	35.385	0.000	0.036	0.362	0.011	0.003	1.373	0.176	0.029	0.568	2.310
BET 4	1.766	0.051	0.107	0.072	0.142	0.001	0.028	0.159	0.106	5.667	21.000

BET 5	0.779	0.038	0.039	0.066	0.075	0.000	0.251	0.262	0.015	4.333	2.010
BET 6	2.260	0.014	0.226	0.143	0.169	0.000	0.003	0.034	0.505	6.729	95.387
BET 7	1.221	-0.041	0.804	0.139	0.178	0.003	0.006	0.022	1.011	7.835	55.089
BET 8	1.766	-0.044	0.721	0.080	0.039	0.002	0.053	0.245	2.237	2.853	15.328
BET 9	4.665	-0.019	0.560	0.078	0.019	0.007	0.169	0.169	0.528	5.382	37.980
BET 10	3.809	-0.050	0.817	0.252	0.063	0.001	0.011	0.188	0.922	5.933	36.457

Keys; **ANK** – Al / (Na + K), • **NKCS** – (Na_2O + K_2O – CaO) / SiO_2, • **CFTMCA** – (CaO + Fe_2O_3T + MgO + TiO_2) / (CaO + Al_2O_3), • **FMAA** – (Fe_2O_3 / (Fe_2O_3 + MgO)) / Al_2O_3, **FMANK** – (Fe_2O_3 / (Fe_2O_3 + MgO)) / (Al_2O_3 + Na_2O + K_2O), **TZR** – TiO_2 / Zr, **NTZ** – Nb / Ta / Zr, **SRRB** – Sr / Rb, **BARB** – Ba / Rb, **RB30** – Rb / 30, **TA3** – Ta × 3

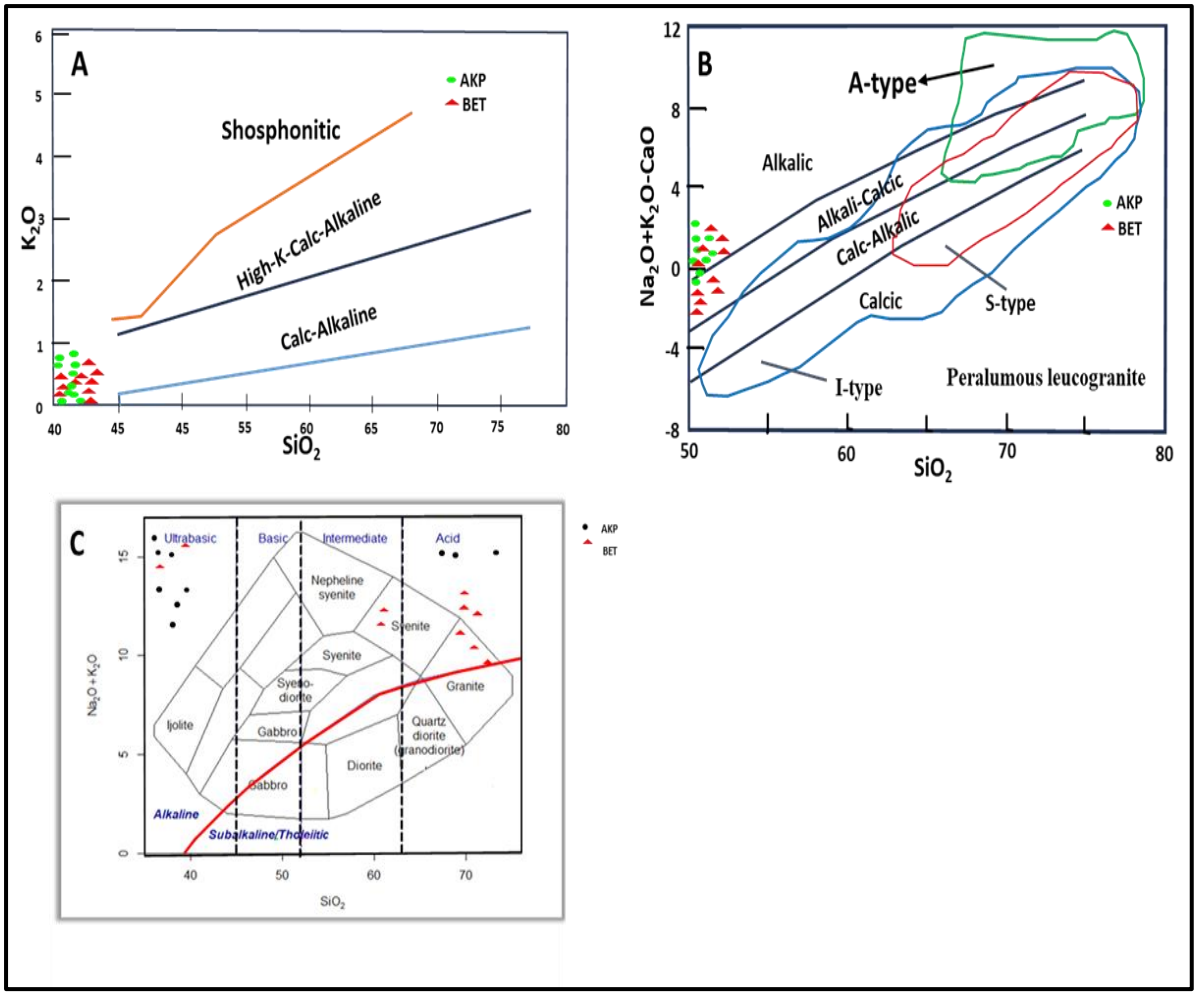

Fig.9. Geochemical diagrams displaying (A) The SiO_2 vs K_2O binary diagram indicates calc-alkaline field characters form Akpet and Betem (after, Peccerillo, & Taylor, 1976); (B) SiO_2 vs Na_2O + K_2O-CaO MALI plot (after Frost et al., 2001) with samples from both areas plotting in the field of alkali to the alkali-calcic field; (C) SiO_2 vs Na_2O + K_2O TAS classification diagram of pegmatites (after Cox *et al.*, 1979).

tend to fall within the alkalic field. This difference implies that the Akpet pegmatites might have undergone a greater degree of magmatic differentiation or were influenced by a slightly different parental magma with a higher alkalic component. Generally, this suggests that while both pegmatites share a common magmatic source, Akpet pegmatites exhibit stronger alkaline enrichment, which could be linked to higher levels of fractionation. On SiO_2 vs Na_2O + K_2O TAS diagram (*Fig.* 9C) of Cox et al., (1979), the compositions of samples from both Akpet and Betem plotted close to the field of alkaline granite. This indicates a higher proportion of alkali metals relative to silica, a feature often associated with certain rock types like basalt and indicative of distinct geological environments (El-Hamed & El-Moneemkabel, 2015). Most of the samples from the Betem area plots in the granodiorite field. This implies that the pegmatites from the Betem area originated from a parent granodioritic melt.

4.3 Protolith, Magmatic Source, and degree of fractionation of the Pegmatites

Determining the protolith of these pegmatites requires evaluating their geochemical affinities. The $CaO+Fe_2O_3T+MgO+TiO_2$ vs. $CaO+Al_2O_3$ plot (*Fig.* 10A) positions the pegmatites from both Akpet and Betem close to the A-type field, indicating a link to highly

fractionated, anorogenic (post-collisional or extensional) granitic melts (Cui, et al., 2022). The $FeO_3/(Fe_2O_3+MgO)$ vs. $Al_2O_3/(Na_2O+K_2O)$ (*Fig.* 10B) plot further refines this classification by placing them in the oxidized A-type field, suggesting a magmatic source that was relatively hot and dry, likely generated in a high-temperature environment with limited water content (Grebennikov, 2014). The TiO_2 vs. Zr plot (*Fig.* 10C) provides further insights into the pegmatite protoliths. Most samples from both Akpet and Betem fall within the S-type granite field, indicating that the pegmatites were primarily derived from the melting of metasedimentary rocks (Finger & Schiller, 2012). However, one sample from the Akpet region plots in the I-type granite field, suggesting a minor contribution from igneous-derived protoliths, possibly a granodioritic or tonalitic source (Orejana, et al., 2012). Results from the discriminant plots indicate that, while the pegmatites from both regions are largely sourced from sedimentary-derived melts, the Akpet pegmatites may have a slightly more diverse origin, possibly involving some input from igneous protoliths.

The molar Na_2O-Al_2O_3-K_2O ternary plot (after Benaouda et al., 2022) was used to discriminate between different types of magmatic compositions, particularly peraluminous, metaluminous, and peralkaline compositions (*Fig.* 10D). This plot utilizes the molar ratios of major oxides, including Na_2O, Al_2O_3, and K_2O, to characterize the chemical characteristics of igneous rocks and infer their petrogenetic origins. Peraluminous rocks are those with an "excess" of alumina (Benaouda et al., 2022). In Betem, a greater number of the samples have lower values of Al_2O_3 content. In contrast, for the Akpet area, a greater number of the samples have higher Al_2O_3 content, indicative of a more peraluminousity nature of pegmatites from this area compared to Betem. Generally, the combined concentration of Al_2O_3 and Na_2O is greater than K_2O. Granites, for example, fall into the peraluminous category. The molar plot of Na_2O-Al_2O_3-K_2O indicated the possible crystallization of the pegmatites from a metaluminous to peraluminous-rich melt. Metaluminous and peraluminous melts, characterized by their aluminum content, offer further insights into the composition of the parental melt from which the pegmatites derived. This suggests that the melt may have been enriched in aluminum
(Feldspar minerals).

The geochemical ratio analysis of the pegmatite samples from Akpet and Betem (as presented in Table 6 and 7) reveals marked contrasts in the degree of fractionation and source rock composition between the two areas. Fractionation indices such as $Al_2O_3/(Na_2O + K_2O)$, $Al_2O_3/(CaO + Na_2O + K_2O)$, and $Fe_2O_3/(Fe_2O_3 + MgO)$ provide insight into the magmatic evolution of the source materials (Yoder, 2015). Akpet samples exhibit significantly higher values, suggesting a more peraluminous and chemically evolved nature, which is indicative of intense weathering and advanced magmatic differentiation. In contrast, the lower values recorded in the Betem samples imply a less evolved character and reduced intensity of fractional crystallization (Yoder, 2015).

The $Fe_2O_3/(Fe_2O_3 + MgO)$ ratio further supports this interpretation. Akpet samples consistently show higher Fe/Mg ratios, reflecting the removal of magnesium-rich ferromagnesian minerals during magmatic evolution and pointing to a higher degree of magmatic fractionation. Betem samples, on the other hand, maintain lower Fe/Mg ratios, characteristic of a less differentiated source (Di Lorenzo and Prieto, 2017). Similarly, the TiO_2/Zr and Rb/Ba ratios, which are commonly used to monitor the behavior of incompatible elements during magmatic processes, show that Akpet is marked by lower TiO_2/Zr values, consistent with greater fractionation. Betem exhibits relatively higher ratios, reinforcing the interpretation of a more primitive source (Larrea et al., 2014). In terms of source rock composition, ratios such as $CaO/(Na_2O + K_2O)$ and $(Na_2O + K_2O - CaO)$ provide clues about the original nature of the rocks. Akpet samples tend to have

lower CaO contents relative to alkalis and often yield negative or low values in the ($Na_2O + K_2O$ - CaO) index, indicating a felsic or crustal source enriched in alkali elements (Shi et al., 2007). This is further supported by elevated Al_2O_3 levels and trace element ratios, such as Nb/Ta/Zr and Rb/Sr, which are commonly associated with crust-derived or reworked sedimentary protoliths (Xiong et al., 2014). In contrast, Betem samples reflect an intermediate composition, with higher CaO contents and trace element ratios suggestive of mantle involvement or derivation from juvenile arc-related material.

4.4 Tectonic Setting and Evolution

The tectonic setting of the pegmatites can be inferred from ternary tectonic classification diagrams (*Fig.* 11A) and trace element discrimination diagrams such as Rb vs. Sr (*Fig.* 11B), Ba vs. Rb (*Fig.* 11C), Nb/Ta vs. Zr (Fig. 11D). The Rb vs. Sr and Ba vs. Rb plots show that pegmatites from both Akpet and Betem fall within the normal granites field, indicating that they are not highly evolved NYF-type pegmatites (Niobium-Yttrium-Fluorine type) but rather granites that underwent moderate differentiation. This suggests a connection to typical granitic intrusions formed during or after major tectonic events (Dill, et al., 2015).

The Nb/Ta vs. Zr plot provides further constraints on tectonic evolution. The pegmatites from both regions exhibit Nb/Ta ratios <10 and Zr values < 100, which are

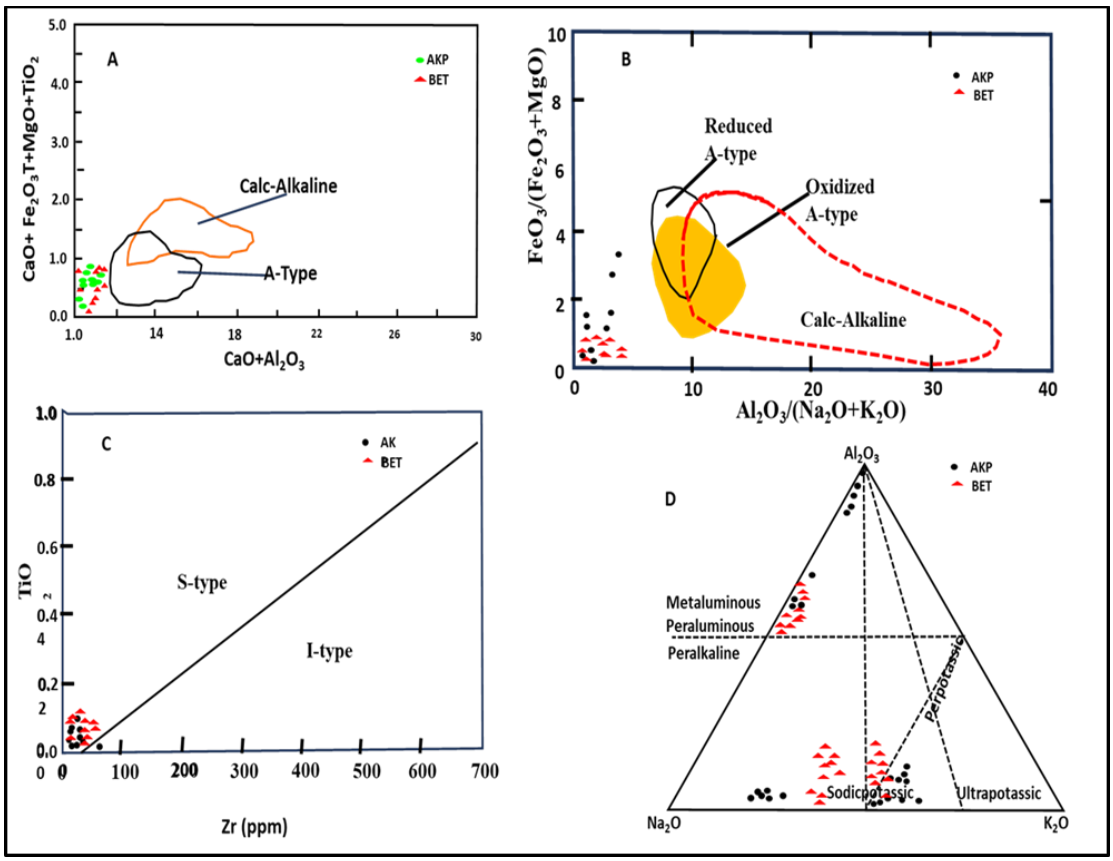

Fig.11. Geochemical diagrams displaying (A): $CaO+Fe_2O_3T+MgO+TiO_2$ vs. $CaO+Al_2O_3$ plot; (B): The $FeO_3/(Fe_2O_3+MgO)$ vs. $Al_2O_3/(Na_2O+K_2O)$; (C): The TiO_2 vs. Zr plot; (D): The molar Na_2O-Al_2O_3-K_2O ternary plot

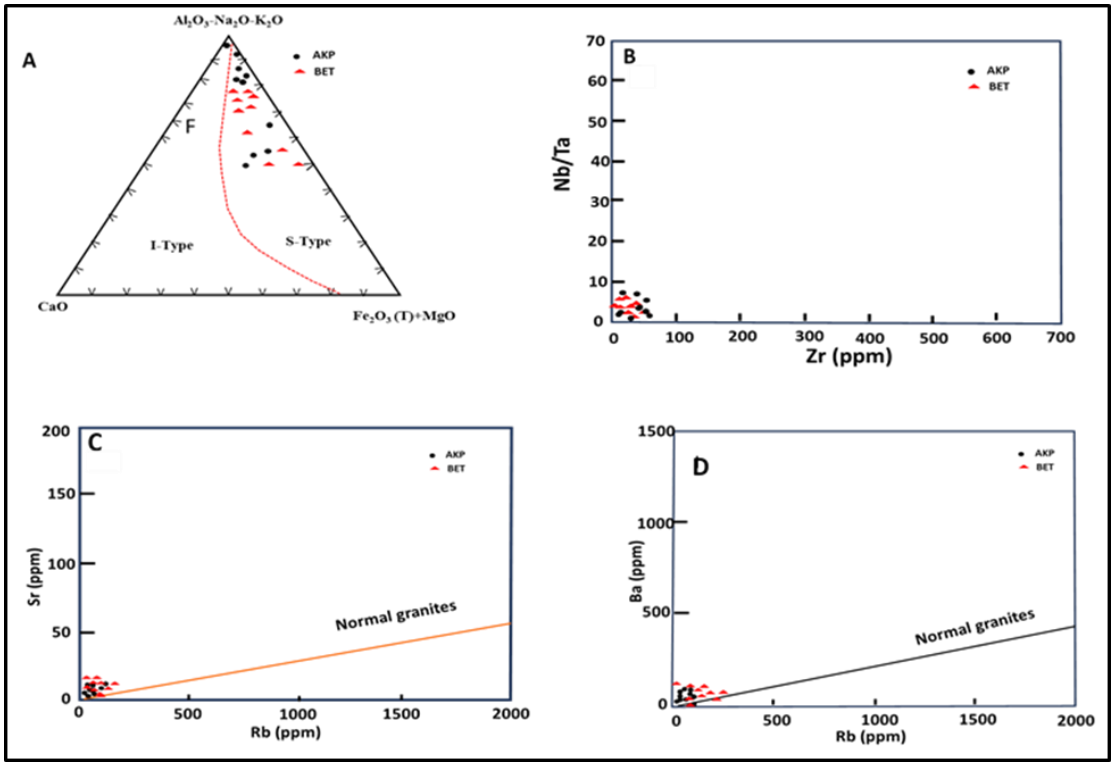

Fig.11. (A) ternary tectonic classification diagrams; trace element discrimination diagrams of (B) Rb vs. Sr, (C) Ba vs. Rb, (D) Nb/Ta vs. Zr depicting tectonic setting for pegmatites from Akpet and Betem

characteristic of crustally derived melts (Martin, et al., 2005; Zozulya, et al., 2022). This is consistent with their S-type affinity, reinforcing the idea that their parental magmas were derived from the partial melting of metasedimentary rocks rather than juvenile mantle-derived magmas. A more detailed insight into the tectonic evolution is provided by the Rb/30, Hf, and Ta*3 ternary diagram, where the samples from both regions plot within the volcanic arc, syn-collision, and within-plate fields (*Fig.* 12). However, the majority of the samples plot in the within-plate field, suggesting that while these pegmatites may have initially formed in a subduction-related or syn-collisional setting, their emplacement likely occurred in a post-collisional, extensional environment (Arikpo et al., 2024). The slightly greater proportion of Akpet samples in the within-plate field suggests that these pegmatites may have undergone a longer period of magmatic differentiation compared to those from Betem. This could be due to prolonged extensional tectonics in the Akpet region, allowing for further melt evolution before final crystallization.

4.5 Comparative analysis of the mineralization potential of pegmatites in Akpet and Betem

The mineralization potential of pegmatites from the two studied areas was carried out using indices of fractionation, such as K/Rb, K/Rb vs. Cs, K/Cs, and K/Ba (*Fig.* 13). According to Wise and Brown (2012), pegmatites form from highly fractionated magmas that have undergone extensive crystal fractionation.This process involves the selective crystallization and settling of minerals from the melt, leading to the enrichment of certain elements in the residual melt that eventually solidifies into pegmatites. Low ratios of K/Rb, K/Cs, and Ta/Cs indicate that the pegmatites are highly fractionated, and thus mineralized. While, higher values indicate that the pegmatites are not highly fractionated, and hence barren

(Edem et al., 2015;Omang et al., 2024). In the present study, the ratios of K/Rb from both Akpet and Betem areas are significantly low indicating that the pegmatites from both areas are highly fractionated and mineralized to Rb. In slight contrast, considerably high K/Cs ratios are observed in two sample stations in Akpet (AKP 1 and AKP 4) having K/Cs values of 80 and 8.3 respectively. Similarly, four sample stations from Betem (BET 3, BET 5, BET 8, and BET 9) recorded very high K/Cs values, an indication of decreasing fractionation in pegmatites from Betem area compared to Akpet. Adetunji and Ocan, (2010), also stated that the K/Rb ratio of pegmatite samples less than a hundred (<100) are mineralized, while those greater than hundred (>100) are barren. Based on the computed results of the indices of fractionation for the analyzed pegmatite samples given in Table 6 and 7, pegmatite samples from both Akpet and Bettem are less than 100 and, hence are highly mineralized.

These plots help differentiate between potentially mineralized and barren pegmatites based on their geochemical composition (Okonkwo and Idakwo, 2020). Commonly used plots include K/Rb vs. Ga (Gallium), K/Rb vs. Rb or K/Rb vs. Cs (to discriminate between barren and potentially mineralized pegmatites), Ta vs. K/Cs (to discriminate tantalite mineralized pegmatites from non-tantalites-bearing pegmatites). In this study, the discrimination plots employed are the K/Rb vs. Rb discrimination plot (Staurov et al., 1969), plot of Ta vs. K/Cs (Beus, 1966), and Be/K/Nb. The K/Rb vs. Rb discrimination plot (*Fig.* 13) reveals that the pegmatites in both Akpet and Betem are mineralized. The Plot of Ta vs. K/Cs (*Fig.* 13A) shows a more variable distribution of mineralization. Six samples (AKP1, AKP3, AKP 4, AKP 5, AKP 8, AKP 10) from Akpet showed low affinity to Ta mineralization. Similarly, four samples (BET3, BET5, BET8, and BET9) showed low affinity for tantalite mineralization

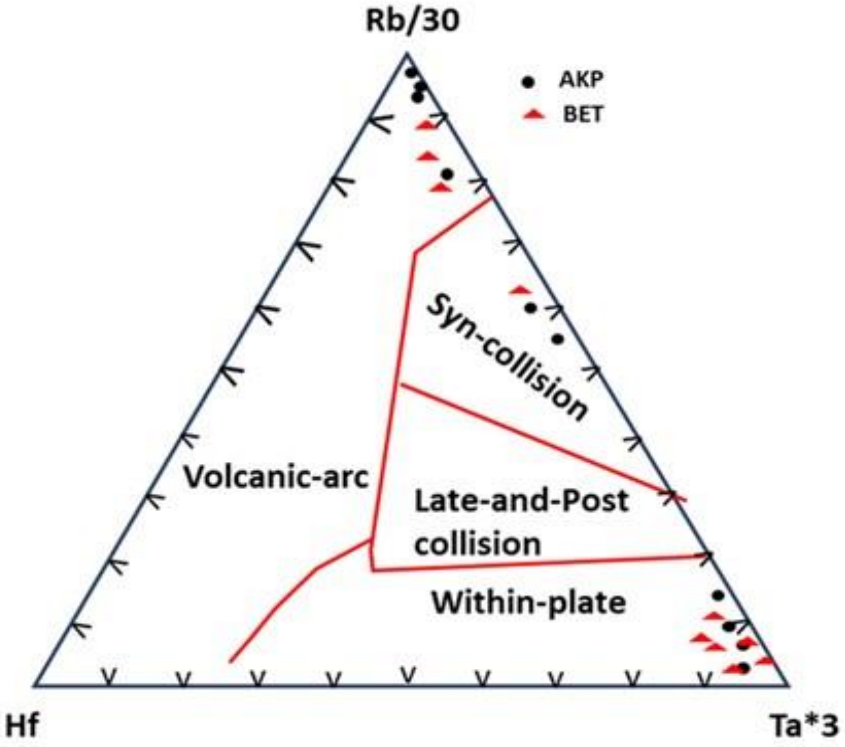

Fig.12. Ternary Hf-Rb/30-Ta*3 diagram

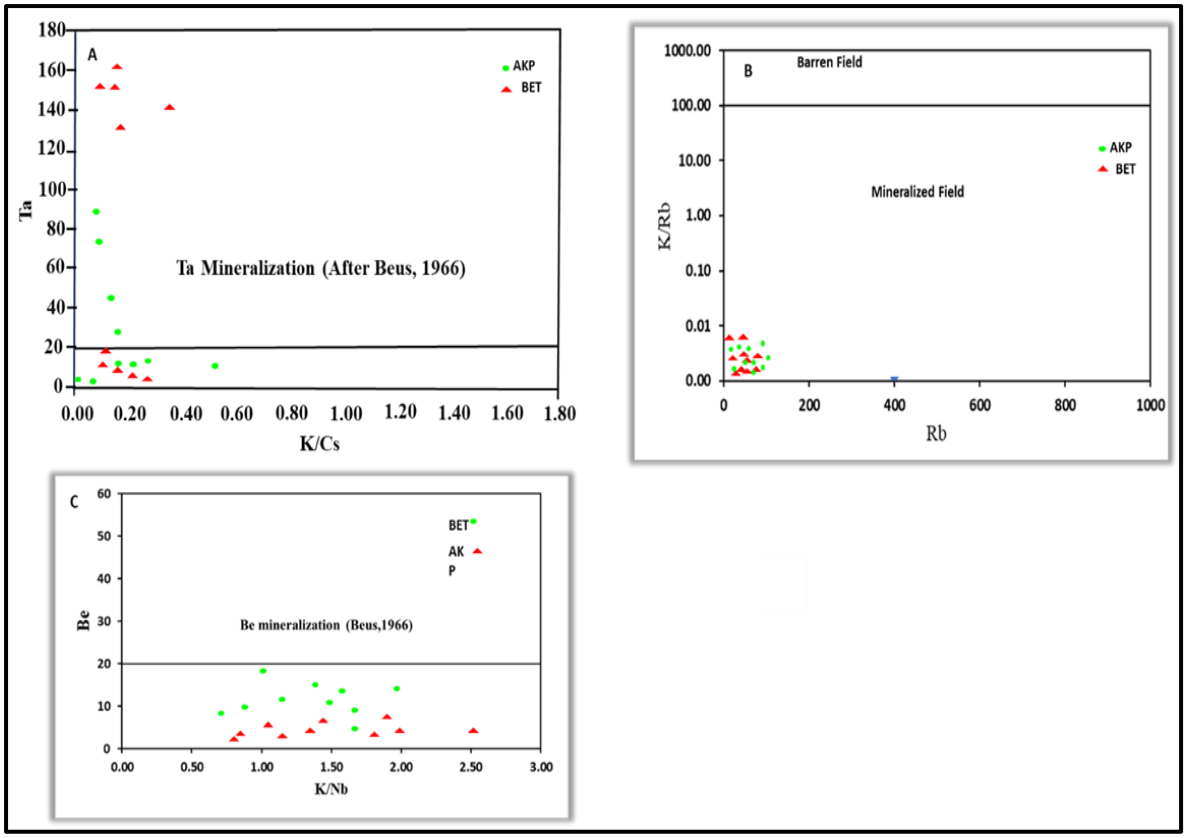

Fig.13. Plot of (A): Ta vs. K/Cs to determine the Tantalum potential of the Akpet and Betem pegmatites (after Beus, 1966); (B) K/Rb vs. Rb distribution pattern in the pegmatites of Akpet and Betem pegmatites showing barren and mineralized pegmatites (fields after Staurov et al., 1969) (C) Plot of Be vs. K/Nb to determine the Beryllium potential of the Akpet and Betem pegmatites (field after Beus, 1966).

(As seen in *Fig.* 13B). The Be/K/Nb plot showed that all the samples from both Akpet and Betem are barren with respect to beryl mineralization (*Fig.* 13C).

5.0 Conclusion

The integrated geochemical and statistical analysis conducted on the lepidolite-bearing pegmatites from Akept and Betem area have provided a comprehensive understanding of their geochemical signatures, mineralogical characteristics, and economic potential. Silica (SiO_2) recorded the highest concentration across the two locations with concentrations ranging from 48.14 to 99.79% with a mean of 80.66% and 70.1 to 98.3 with a mean of 82.080%wt for Akpet and Betem areas respectively. Major oxides such as SiO_2, Al_2O_3, K_2O, and Na_2O were enriched, while CaO, MnO, MgO, and TiO_2 were depleted, highlighting the role of fractional crystallization in their petrogenesis and suggesting favorable conditions for lithium mineralization.

The SiO_2 versus K_2O diagram indicates a calc-alkaline affinity for both localities, reflecting a convergent plate margin setting and suggesting derivation from a subduction-modified lithospheric source. The SiO_2 versus (Na_2O+K_2O)–CaO plot places samples in the calcic-alkali to alkalic fields, with Akpet pegmatites showing a stronger alkaline enrichment, implying higher levels of magmatic fractionation.

The protolith discriminant plots revealed that although the pegmatites from both regions are largely sourced from sedimentary- derived melts, the Akpet pegmatites may have a slightly more diverse origin, possibly involving some input from igneous protoliths. Trace element and rare earth element analysis revealed high concentrations of Co, Rb, Cu,

Ni, and Zn in Akpet pegmatites, while Betem pegmatites were highly enriched in Rb, Ba, Zn, and Co. The pegmatites exhibit significant tantalum and rubidium mineralization, although beryllium appears to be absent. Given the association of tantalite with lithium-bearing minerals such as spodumene and lepidolite, these pegmatites represent promising targets for lithium exploration. Multivariate statistical analysis confirmed high degrees of crystallization and differentiation, further supporting the potential for lithium concentration during late-stage magmatic processes.

Given the limited sample size of twenty samples, future studies should involve a larger and more representative dataset to improve the statistical robustness of the geochemical interpretations. To enhance predictive capabilities, future research should integrate machine learning and metaheuristic modeling approaches alongside traditional multivariate statistical tools. Additionally, geophysical methods such as magnetic and electrical resistivity surveys should be incorporated to complement geochemical data and provide a more comprehensive characterization of the pegmatite bodies. These improvements will strengthen the understanding of the genesis, extent, and mineralization potential of lepidolite-bearing pegmatites in southeastern Nigeria.

Acknowledgement

The aurthors wishes to appreciate Dr. Michael Omeka for his invaluable support in writing this research paper.

6.0 References

Arikpo, T. O., Morphy, M. I., Amah, G., Omang, B. O., & Tijani, O. L. (2024). Geochemistry of Awi Sandstone, Calabar Flank, Southeastern (Se) Nigeria: Constraints On The Metal Enrichment, Provenance, And Tectonic Setting. *Global Journal of Geological Sciences*, *22*(1), 79-112.

Aydin, F. (2008). Contrasting complexities in the evolution of calc-alkaline and alkaline melts of the Nigde volcanic rocks, Turkey: textural, mineral chemical and geochemical evidence. *European Journal of Mineralogy*, *20*(1), 101-118.

Benaouda, R., Kraemer, D., Bejtullahu, S., Mouttaqi, A., & Bau, M. (2022). Occurrence of high-grade LREE allanite-pegmatites and calcite carbonatite dykes in the Ediacaran complex of Aghracha, Oulad Dlim massif (South Morocco). *Journal of African Earth Sciences*, *196*, 104727.

Benchmark Mineral Intelligence. (2023). *The Rise of Lithium: A Global Energy Storage*.

Beus, A. A. (1966). *Geochemistry of Beryllium: And Genetic Types of Beryllium Deposits*. WH Freeman.

Cahen, L. (1982). Geochronological correlation of the Late Precambrian sequences on and around the stable zones of Equatorial Africa. *Precambrian Research*, *18*(1-2), 73-86.

Černý, P., & Ercit, T. S. (2005). The classification of granitic pegmatites revisited. *The Canadian Mineralogist*, *43*(6), 2005-2026.

Cox, K. G. (Ed.). (2013). *The interpretation of igneous rocks*. Springer Science & Business Media.

CRU Group. (2023). *The Future of Lithium: Supply, Demand, and Price Forecasts*. CRU Group.

Cui, X., Sun, M., & Zhao, G. (2022). Syn-orogenic A-type granites and post-collisional I-type granite in the southern Chinese Altai: Petrogenesis and implications for granite classification. *Gondwana Research*, *111*, 20-34.

Dharmapriya, P. L., Disanayaka, D. W. M., Pitawala, H. M. T. G. A., Malaviarachchi, S. P., & Subasinghe, N. D. (2025). Genesis, Classification, Tectonic Setting and Economic Potential of Global Granitic Pegmatites: A Review. *Evolving Earth*, *100059*.

Dill, H. G., & Dill, H. G. (2015). Pegmatites and Their Country Rocks in the Central European Variscides. *The Hagendorf-Pleystein Province: the Center of Pegmatites in an Ensialic Orogen*, 111-172.

Dill, H. G. (2015). Pegmatites and Aplites: Their Genetic and Applied Ore Geology. *Ore Geology Reviews*, *69*, 417–456. https://doi.org/10.1016/j.oregeorev.2015.02.022

Di Lorenzo, F., & Prieto, M. (2017). Dissolution–recrystallization of (Mg, Fe) CO3 during hydrothermal cycles: FeII/FeIII conundrums in the carbonation of ferromagnesian minerals. *Crystal Growth & Design*, *17*(8), 4170-4182.

Edem, G. O., Ekwueme, B. N., & Ephraim, B. E. (2015). Geochemical signatures and mineralization potentials of precambrian pegmatites of southern Obudu, Bamenda Massif, southeastern Nigeria. *International Journal of Geophysics and Geochemistry*, *2*(3), 53-67.

Ekwueme, B. N. (1987). Structural orientations and Precambrian deformational episodes of Uwet area Oban massif, SE Nigeria. *Precambrian Research*, *34*(3-4), 269-289.

Ekwueme, B. N. (1990). Rb-Sr ages and petrologic features of Precambrian rocks from the Oban Massif, southeastern Nigeria. *Precambrian Research*, *47*(3-4), 271-286.

Ekwueme, B. N. (1995). The Nature of Magmatism and Tectonic Setting of the Oyioba-Uganga Area, Southern Benue Trough, Nigeria: Evidence from Major and Trace Element Geochemistry. *Magmatism in Relation to Diverse Tectonic Settings*, 67-77.

El Bouseily, A. M., & El Sokkary, A. A. (1975). The relation between Rb, Ba and Sr in granitic rocks. *Chemical Geology*, *16*(3), 207-219.

EL-MEZAIN, A. H. M. E. D., MOHAMED OMAR, S. A. Y. E. D. A. H. M. E. D., EL-HAMED, M. E. D., & EL-MONEEMKABEL, A. E. F. (2015). GEOLOGY, PETROGRAPHY, GEOCHEMISTRY AND SUITABILITY OF ABU SHEIH PEGMATITE FOR CERAMIC INDUSTRY. *Al-Azhar Bulletin of Science*, *26*(1-D), 91-108.

Ercit, T. S., Linnen, R. L., & Samson, I. M. (2005). REE-enriched granitic pegmatites. *Rare-Element Geochemistry and Mineral Deposits: Geological Association of Canada, GAC Short Course Notes*, *17*, 175-199.

Ero, K. A., & Ekwueme, B. N. (2009). Mineralization of pegmatites in parts of the Oban Massif, Southeastern Nigeria: A preliminary analysis. *Chinese Journal of Geochemistry*, *28*(2), 146–153. https://doi.org/10.1007/s11631-009-0146-2

Finger, F., & Schiller, D. (2012). Lead contents of S-type granites and their petrogenetic significance. *Contributions to Mineralogy and Petrology*, *164*, 747-755.

Frost, B. R., Barnes, C. G., Collins, W. J., Arculus, R. J., Ellis, D. J., & Frost, C. D. (2001). A geochemical classification for granitic rocks. *Journal of Petrology*, *42*(11), 2033-2048.

Gao, Y., Bagas, L., Li, K., Jin, K., Liu, Y., & Teng, J. (2020). Newly discovered Triassic lithium deposits in the dahongliutan area, north west China: A case study for the detection of lithium-bearing pegmatite deposits in rugged terrains using remote-sensing data and images. *Frontiers in Earth Science*, *8*, 591966. https://doi.org/10.3389/feart.2020.591966

Gardiner, N. J., Jowitt, S. M., & Sykes, J. P. (2024). Lithium: critical, or not so critical? *Geoenergy*, *2*(1), geoenergy2023-045.

Groves, D. I., Zhang, L., Groves, I. M., & Sener, A. K. (2022). Spodumene: The key lithium mineral in giant lithium-cesium-tantalum pegmatites. *Acta Petrologica Sinica*, *38*, 1–8. https://doi.org/10.18654/1000-0569/2022.01.01

Gupta, C. K., & Krishnamurthy, N. (2005). *Extractive Metallurgy of Rare Earths*. CRC Press.

Kesler, S. E., Gruber, P. W., Medina, P. A., Keoleian, G. A., Everson, M. P., & Wallington, T. J. (2012). Global lithium resources: Relative importance of pegmatite, brine and other deposits. *Ore Geology Reviews*, *48*, 55-69.

Krishna Kumar, S., Bharani, R., Magesh, N. S., Godson, P. S., & Chandrasekar, N. (2014). Hydrogeochemistry and groundwater quality appraisal of part of south Chennai coastal aquifers, Tamil Nadu, India using WQI and fuzzy logic method. *Applied Water Science*, *4*, 341-350.

Larrea, P., Galé, C., Ubide, T., Widom, E., Lago, M., & França, Z. (2014). Magmatic evolution of graciosa (Azores, Portugal). *Journal of Petrology*, *55*(11), 2125-2154.

Li, B., Zhao, L., Lu, A. H., Luo, J. B., Kong, H., & Lai, J. Q. (2024). Mineralogical constraints on pegmatite genesis and rare metal mineralization in the Mufushan batholith, South China. *Ore Geology Reviews*, *164*, 105856.

Linnen, R. L., Lichtervelde, M. V., & Cerny, P. (2012). Granitic Pegmatites as Sources of Strategic Metals. *Elements*, *8*, 275–280. https://doi.org/10.2113/gselements.8.4.275.

London, D. (2008). *Pegmatites*. Can. Mineral. Spec. Publ.

Martin, R. F., & De Vito, C. (2005). The patterns of enrichment in felsic pegmatites ultimately depend on tectonic setting. *The Canadian Mineralogist*, *43*(6), 2027-2048.

Meshram, R. R., Singh, B., Mishra, M. K., Hrushikesh, H., Siddiqui, A., Shukla, D., Meshram, T. M., & Geological Survey. (2021). Petrological and Geochemical Studies of Lepidolite (LCT Type) and Non-Lepidolite Pegmatite's from Chakrasila, Dhubri District, Assam, North East India. *Open Journal of Geology*, *11*(3), 81-104.

Muller, A., Reimer, W., Wall, F., Williamson, B., Menuge, J., Brönner, M., et al. (n.d.). *Mineralogical characterization of Gidan Jaja iron ore, Zamfara State, Nigeria*.

Mustapha, A. (2012). Application of principal component analysis & multiple regression models in surface water quality assessment. *Journal of Environmental Science*, *2*(2), 16–23.

Obiora, S. C. (2006). Petrology and geotechnic setting of the basement comple rocks around Ogoja, South-Eastern Nigeria. *Ghana Journal of Science*, *46*, 13-25.

Oden, M. I., & Igonor, E. E. (2012). The Behaviour of Feldspar Megacrysts in Granitic Pegmatite Veins Western Oban Massif, Nigeria. *Advances in Applied Science Research*, *3*(2), 1880-1888.

Omang, B. O., Njoku, A. K., Arikpo, T. O., & Kave, G. T. (2025). Geochemistry of the Ironstones in Abiati Area, Southeastern Nigeria: Implications for Ore Genesis and Economic Potential. *Communication In Physical Sciences*, *12*(3), 880-913.

Omang, B. O., Morphy, M. I., Amah, G., Tijani, O. L., Arikpo, T. O., & Kave, G. T. (2024). Major And Trace Element Geochemistry Of Pegmatites In Umai, Oban Massif, Se, Nigeria: Constraints On Their Characterization And Mineralization Potential. *Global Journal of Geological Sciences*, *22*(1), 125-145.

Omeka, M. E., Amah, G., Morphy, M. I., Omang, B. O., Asinya, E. A., & Kave, G. T. (2024). A systematic review on the trends, progresses, and challenges in the application of artificial intelligence in water quality assessment and monitoring in Nigeria. *Global Journal of Pure and Applied Sciences*, *30*(4), 447-470.

Orejana, D., Villaseca, C., Valverde-Vaquero, P., Belousova, E. A., & Armstrong, R. A. (2012). U–Pb geochronology and zircon composition of late Variscan S-and I-type granitoids from the Spanish Central System batholith. *International Journal of Earth Sciences*, *101*, 1789-1815.

Peccerillo, A., & Taylor, S. R. (1976). Geochemistry of Eocene calc-alkaline volcanic rocks from the Kastamonu area, northern Turkey. *Contributions to Mineralogy and Petrology*, *58*, 63-81.

Shen, P., Pan, H., Li, C., Feng, H., He, L., Bai, Y., et al. (2022). Newly-recognized Triassic highly fractionated leucogranite in the Koktokay deposit (Altai, China): Rare-metal fertility and connection with

the No. 3 pegmatite. *Gondwana Research*, *112*, 24–51. https://doi.org/10.1016/j.gr.2022.09.007

Shi, C., Yan, M., & Chi, Q. (2007). Abundances of chemical elements of the granitoids in different geotectonic units of China and their characteristics. *Frontiers of Earth Science in China*, *1*, 309-321.

Taylor, A. P. (1974). *The Geology of an Archaean Nickel Sulphide Occurrence, Western Australia* [Doctoral dissertation, The University of Manchester]. The University of Manchester (United Kingdom).

Thomas, R., & Davidson, P. (2012). Water in granite and pegmatite-forming melts. *Ore Geology Reviews*, *46*, 32-46.

U.S. Geological Survey. (2023). *Mineral Commodity Summaries 2023: Lithium*. U.S.

Ulmer, P. (2007). Differentiation of mantle-derived calc-alkaline magmas at mid to lower crustal levels experimental and petrologic constraints. *Periodico di Mineralogia*, *76*(2-3), 309-325.

Wise, M., & Brown, C. D. (2012). Mineral chemistry, petrology and geochemistry of the Sebago granite-pegmatite system, southern Maine, USA. *Journal of GEOsciences*, *3–26*. https://doi.org/10.3190/jgeosci.061.

Xiong, F., Ma, C., Zhang, J., Liu, B., & Jiang, H. A. (2014). Reworking of old continental lithosphere: an important crustal evolution mechanism in orogenic belts, as evidenced by Triassic I-type granitoids in the East Kunlun orogen, Northern Tibetan Plateau. *Journal of the Geological Society*, *171*(6), 847-863.

Yoder Jr, H. S. (2015). *Evolution of the igneous rocks: Fiftieth anniversary perspectives*. Princeton University Press.

Zhang, X., Aldahri, T., Tan, X., Liu, W., Zhang, L., & Tang, S. (2020). Efficient coextraction of lithium, rubidium, cesium and potassium from lepidolite by process intensification of chlorination roasting. *Chemical Engineering Processing: Process Intensification*, *147*, 107777. https://doi.org/10.1016/j.cep.2019.107777

Zozulya, D., Macdonald, R., Bagiński, B., & Jokubauskas, P. (2022). Nb/Ta, Zr/Hf and REE fractionation in exotic pegmatite from the Keivy province, NW Russia, with implications for rare-metal mineralization in alkali feldspar granite systems. *Ore Geology Reviews*, *143*, 104779.

Declarations

The authors declare that they have no conflict of interest.

Data availability

All data used in this study will be readily available to the public.

Consent for publication

Not Applicable

Availability of data and materials

The publisher has the right to make the data Public.

Competing interests

The authors declared no conflict of interest.

Funding

There is no source of external funding

Author contributions

BOO, conceptualize and reviewed the manuscript. UNN, and TOA wrote and arranged the manuscript. UO and DTK, revised the manuscript.